THE ASTROPHYSICAL JOURNAL, 405:8–29, 1993 March 1

LIMITS ON THE ANISOTROPY OF THE MICROWAVE BACKGROUND RADIATION ON ARCMINUTE SCALES. II. THE RING EXPERIMENT

S. T. MYERS,[1] A. C. S. READHEAD, AND C. R. LAWRENCE
Owens Valley Radio Observatory, California Institute of Technology, Pasadena, CA 91125
Received 1992 February 21; accepted 1992 August 31

ABSTRACT

Observations at a frequency of 20 GHz with the Owens Valley Radio Observatory 40 m telescope are used to place limits on the anisotropy of the cosmic microwave background radiation on arcminute angular scales. The new experiment, designated the RING, consists of a survey of 96 fields at declination $\delta = 88°10'42''$, observed in an interlocked ringlike geometry that provides improved discrimination against systematic biases and allows reconstruction of the intrinsic fluctuations from the differenced data. The RING experiment has high sensitivity for a variety of non-Gaussian fluctuation models but is susceptible to contamination by discrete extragalactic radio sources. Where possible, lower frequency VLA observations were used to identify and correct for the contributions of these objects. Statistical analysis of the RING data results in detections of anisotropy of $2.3 < \Delta T/T < 4.5 \times 10^{-5}$ (95%) and $1.6 < \Delta T/T < 6.1 \times 10^{-5}$ (99.87%), assuming $T_{\rm mwb} = 2.735$ K, for Gaussian fluctuations that are uncorrelated between the RING fields. The amplitude of these fluctuations is significantly higher than that predicted for CDM models consistent with the recent *COBE* results and is also inconsistent at the 95% confidence level with earlier measurements using the same instrument. Because of the high likelihood of residual radio source contamination, these detections are treated as upper limits on intrinsic background fluctuations. Of the 96 RING fields, seven fields were found to have signals of 3 σ or greater, and four of these were subsequently shown to be contaminated with extragalactic nonthermal radio sources. One of the remaining fields, which exhibits a 5 σ fluctuation, has not been identified with any known foreground source and is the best candidate field for a background fluctuation, although foreground contamination has not been ruled out. In conjunction with previous observations, we find $\Delta T/T < 10^{-4}$ for Gaussian fluctuations with correlation angles between 0.7 and 7′ (95%). Implications for cosmology and theories of galaxy formation are discussed.

Subject headings: cosmic microwave background — cosmology: observations — galaxies: formation — radio continuum: general

1. INTRODUCTION

The isotropy of the cosmic microwave background radiation beyond the dipole component has been perhaps the most important yet perplexing result to emerge from observational cosmology in the 27 years since its discovery. It is hoped that intrinsic (or primary) fluctuations observed in this background will provide a crucial link between the wealth of structure in the distribution of matter that we see around us today and conditions in the early universe. Since the experiments of Uson & Wilkinson (1984a, b, c) and the interpretation of their results in the context of galaxy formation models by Bond & Efstathiou (1984) and Vittorio & Silk (1984), the upper limits have been steadily approaching the 10^{-5} level over a wide range of angular scales, placing ever-tighter limits on the parameter space available to theorists in construction of models.

On the largest angular scales, all-sky surveys from space and the upper reaches of the atmosphere have provided detailed maps of the microwave background. Results from the *RELIKT-1* (Klypin et al. 1987) spacecraft and the first reports from the *COBE* satellite differential microwave radiometer (DMR) experiment (Smoot et al. 1991) placed upper limits of 3×10^{-5} on the quadrupole component. (The most important observation to date regarding microwave background anisotropy is, of course, the recent detection of fluctuations from the *COBE* satellite [Smoot et al. 1992]. Because these results were announced after submission of this paper, the implications of the *COBE* measurement with regard to the experiment reported here will be discussed in § 7 at the conclusion of this manuscript.) Balloon-based experiments (Bernstein et al. 1989; de Bernardis et al. 1990; Boughn et al. 1992; Meyer, Cheng, & Page 1991) have also placed stringent limits on low-order multipoles of the background field. There was a report of a possible detection of fluctuations on an angular scale of 8° (Davies et al. 1987) at a level of 3.7×10^{-5} consistent with contamination expected due to galactic synchrotron emission (Banday & Wolfendale 1990; Banday et al. 1991), thus illustrating the problems facing experimenters due to foregrounds.

Ground-based experiments have been successful at intermediate and smaller angular scales. Interferometric observations from Timbie & Wilkinson (1988, 1990) place limits on degree-scale anisotropy of 2×10^{-5}. Observing from the South Pole, Meinhold & Lubin (1991) have results on angular scales from 20′–1° ($\delta T/T < 3.5 \times 10^{-5}$ on 20′), with improved sensitivity expected soon. On arcminute angular scales, the Caltech program has produced an eight field high-sensitivity experiment (Readhead et al. 1989), with an upper limit of 1.9×10^{-5} for fluctuations with a characteristic coherence scale of 2.6. Limits were set on subarcminute-scale anisotropy using the VLA (Martin & Partridge 1988; Fomalont et al. 1988; Hogan & Partridge 1989) near the 10^{-4} level, while new limits (Fomalont et al. 1992) press down to the 1.9×10^{-5} level.

[1] Also Canadian Institute for Theoretical Astrophysics, Toronto, ON, Canada M5S 1A7.

The status of observations on angular scales $\leq 20°$ has recently been reviewed by Readhead & Lawrence (1992).

Up until this time, the arcminute-scale experiments have examined only a small number of sample regions. A calculation of the optimal number of fields (Readhead et al. 1989, Appendix) shows that maximum sensitivity to Gaussian fluctuations is obtained for 14–25 fields and decreases slowly as the number is increased. However, fluctuations produced by many non-Gaussian distributions are more likely to be detected with a larger number of fields, as the increased probability of tail events makes up for decreased single-field sensitivity. As an example, simply inducing nonrandom phase correlations in the temperature distribution through the introduction of "voids" (regions with an absence of fluctuations) will greatly reduce the expected signal for smaller experiments. Confusion from discrete radio sources unfortunately also increases with survey area for the same reason, and larger data sets will suffer more from contamination.

While the eight field "NCP" program of Readhead et al. (1989, hereafter Paper 1) obtained high sensitivity for Gaussian fluctuations by focusing on a restricted number of fields, the limited area of sky coverage (~ 0.017 deg^2) is poor for probing non-Gaussian models. The experiment described in this paper, designated as the "RING," covers ~ 0.1 deg^2 and extends the area by a factor of 6 while maintaining good sensitivity to Gaussian fluctuations. Most important, the observing geometry was selected to enable the reconstruction of individual field amplitudes from the difference data points and to provide discrimination against many kinds of systematic errors. The dry desert site of the Owens Valley Radio Observatory and the availability of the 40 m telescope allow the accumulation of the hundreds of hours of observing time required to achieve sensitivity levels around 100 μK per field. In this paper data from 1986–1990 are used to obtain anisotropy limits on angular scales from 1′–10′ of $< 1.4 \times 10^{-4}$, and $< 5 \times 10^{-5}$ at 2.6 (95% confidence). The presence of a signal in the data is attributed to contamination by foreground nonthermal extragalactic radio sources, using extrapolated source counts and direct VLA measurements. We find two candidate fields in which no objects were detected with the VLA yet remain larger than 3 σ in the RING. We discuss the limits placed on Gaussian and non-Gaussian models by these results.

2. OBSERVATIONS

The experimental configuration and most of the observing details used for the RING are identical to those used in the eight field NCP experiment presented in Paper 1. We summarize the observing procedure and point out the features that differ from those for the NCP program. Additional details of the RING observations are given in Myers (1990).

The number of target fields chosen was 96, providing a large increase in the area coverage over the previous program yet allowing us to reach similar sensitivity levels in a few hundred hours of integration time. The 96 fields form a linked ring at $\delta = 88°10'42''$ with a spacing of 15^m in right ascension equivalent to the 7.15 separation between beams on the switched receiver (Fig. 1). The R.A. of field i is $\alpha_i = (i - 1)\ 15^m$. These positions are given in mean coordinates of epoch 1987.0. The fields are designated NPR*hhmm* (for North Polar Ring), where *hhmm* denotes the right ascension in hours and minutes.

In the RING geometry, the reference beams in the double switching pattern for one field are nearly coincident with the main beams for adjacent fields. The switched measurement for RING field i is thus, using the notation of Paper 1,

$$\begin{aligned} \Delta T_i &= T_M - \tfrac{1}{2}(T_{R1} + T_{R2}) , \\ &\approx T_i - \tfrac{1}{2}(T_{i-1} + T_{i+1}) , \end{aligned} \tag{1}$$

where the leading and trailing reference fields $R1$ and $R2$ are identified with the adjacent RING field main beams. With this scheme, real sources will show up with a characteristic minus-plus-minus pattern in consecutive fields. In addition, the expected overall sum of field levels is zero, giving an important check on systematic errors. Because the fields are located on a circle of constant declination while the switching is done in azimuth, the true position of the reference beams is 0.24 south of the adjacent field centers. As this is a small fraction of a beam width, the RING interlock error will have little effect on sources near the center of the beams and extended sources, but poses potential problems for point sources outside the half-power response level.

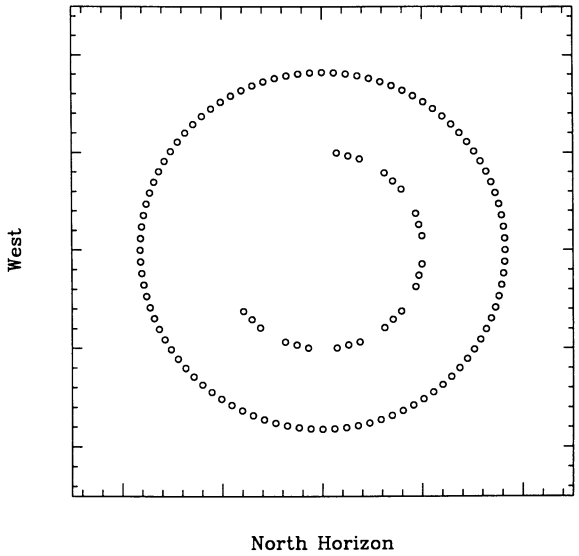

FIG. 1.—Approximate projection of RING (outer circles) and NCP (inner circles) field centers on the sky. Orientation is such that the North horizon (azimuth = 0) lies toward the bottom and West is to the left. The spacing between tick marks is 0.2. The field NPR0000 is the uppermost in the outer circle, NCP1 is at the top of the inner. R.A. increases clockwise from zero at top. The size of the open circle markers is approximately twice the OVRO primary beam FWHM 1.8.

2.1. *Setup and Calibration*

As in the previous work (Paper 1), the 40 m telescope at OVRO was used with the K-band maser receiver at an observing frequency of 20 GHz with a 400 MHz bandwidth. On any given day, each field was observed for only 12 minutes centered at transit. The individual integrations (denoted as FLUXes) were taken in a double switching pattern with Dicke switching between the horns at 10 Hz followed by moving of the antenna on the sky by the beam separation. The second switching was performed in the standard off-on-on-off pattern with a single FLUX measurement completed in a total cycle time of 40 s, a rate twice as fast as that used in the NCP observations of Paper 1. This change was made to obtain a reasonable number of samples during a single 12 minute scan to define noise statistics. As before, noise was injected in the main beam side of the signal path to compensate for an imbalance in the power

levels in the two arms; the amplitude was periodically adjusted to produce equal power output at the radiometer in the two channels. During the observations reported here, the magnitude of the added noise was approximately 5 K and varied diurnally by 0.1–0.4 K. Because diurnal signals are reduced by a factor of $\sim 4 \times 10^6$ by the double switching, a maximum effect of only 0.1 μK is expected for the RING data. Later examination of the receiver waveguide located a loose flange, which when repaired removed the imbalance between the main beam and reference channels.

The observing schedule was set up so that a cycle consists of pointing and calibration on the nearby source (1637+826) followed by observations of three RING fields. Every hour, a pointing scan on the calibrator was substituted for one of the RING field observations, and each day a different field was replaced. Thus, in four days, each of the RING fields would be observed three times. A scan on a field began with integrations of the total power and Dicke-switched outputs (for later diagnostics on the level of the signals) and a record of the wind speed. A 40 second off-on-on-off measurement of the small calibration diode (LCAL) was made, followed by a series of FLUX measurements. The scan was stopped 6 minutes after transit, and the observations on the next field (or calibrator) begun.

Several quantities must be measured to ensure proper calibration of the data. These are the equivalent temperatures of the large (HCAL) and small (LCAL) noise diodes, the aperture and beam efficiencies, the system temperatures of the various components of the receiver, and the gain of the telescope as a function of zenith angle. The absolute calibration of the HCAL was performed using hot and cold absorbing loads. The system gain was monitored during the data acquisition using the LCAL. These parameters were linked using the ratio of large to small diode powers, which was monitored frequently. Also, the flux densities of a set of reference radio sources relative to the CAL sources were measured regularly to allow a check on the temperature scale. For calibration purposes, we split the observations into three separate ranges: 1986 December 1–1987 April 23, 1988 November 26–1989 January 3 (plus calibration sessions during 1988 August 30–September 1 and October 6–9), and the period from 1989 January 18 onward. The division into these intervals was necessitated by the work done on the maser receiver package in 1987–1988 and the installation of a new second stage amplifier and refrigerator overhaul (requiring disassembly of the noise source injection assembly) in 1989 January, both of which caused changes in the coupling of the HCAL and LCAL into the front-end waveguides. Although the NCP and RING programs overlapped in the 1986–1987 session, system parameters were determined independently whenever possible, and agreement verified.

To find the sensitivity of the *K*-band system on the 40 m telescope (in Jy K^{-1}) we use the measured flux densities of two standard sources, DR 21 and NGC 7027. Both are nonvariable Galactic objects. The flux density of DR 21 is derived using the scale near $\lambda = 1$ cm from Klein & Gulkis (1978) giving us a value of 19.4 $\pm$ 0.6 Jy at 20 GHz. The flux density of NGC 7027 is given as 5.9 $\pm$ 1.3 Jy (Baars et al. 1977), but we choose to refer directly to DR 21. We have measured both NGC 7027 and DR 21 on five occasions and determined the ratio NGC 7027/DR 21 = 0.315 $\pm$ 0.004, and thus we derived 6.11 $\pm$ 0.20 Jy for the flux density of NGC 7027, in agreement with the Baars et al. value. From the error bars on the two values, we estimate an overall uncertainty of 3% in the flux density scale. The gain of the 40 m antenna as a function of zenith angle was determined by tracking a bright radio source such as DR 21 or 3C 84 over a large range of zenith angles. Correction for atmospheric absorption was made using the optical depth determined by measuring the antenna temperature as a function of zenith angle and comparing this with the temperature of the water vapor emission. For the weather conditions under which the calibrators were observed, we find a mean correction factor of 4.5% $\pm$ 1.3% for the zenith angle at which the gain was normalized. Combining the measurements of the flux and temperature of the CAL sources we find a sensitivity $\xi = 7.99 \pm 0.26$ Jy K^{-1}. This corresponds to an aperture efficiency (see Kraus 1982) of $\eta_a = 0.280 \pm 0.009$ for a 130 foot (40 m) diameter aperture, consistent with the value 0.27 $\pm$ 0.01 adopted in Paper 1. Finally, we can use the sensitivity ξ along with the derived $S_{\rm LCAL}$ in the first session to calculate the appropriate values for noise diode temperatures. Our final calibrated equivalent temperatures along with important system parameters are summarized in Table 1.

The thermodynamic equivalent temperatures are related to the sky brightness temperature T_i as seen in the main beam of the switched RING integration ΔT_i through correction factors for atmospheric absorption, main beam efficiency, and the Rayleigh-Jeans approximation to the blackbody function. At the zenith angle of the RING observations (50°.9) and for the optical depth during the superior weather under which the RING was observed, there is a 1.044 $\pm$ 0.013 correction factor for atmospheric absorption. In addition, the measured antenna temperatures include radiation received through the sidelobes of the telescope response pattern in addition to the main beam directed at the target sources. This "spillover" radiation consists of components from both the sky and ground which are common to the two beams and thus cancel in the differenced measurements (as evidenced by the zero RING mean level seen in § 3). Because our temperature calibration is referenced to a thermal load filling the entire beam, we underestimate the true sky temperature by the ratio of the main beam area to the total beam solid angle $\eta_B = 0.47 \pm 0.02$ (Paper 1). Finally, we make a 1% correction for the true blackbody $\partial B_\nu/\partial T$ for 3 K at 20 GHz. We combine all of the correction factors detailed above into a single multiplicative factor $\kappa = 2.22 \pm 0.10$, which is then applied to the FLUX measurements Δt_i^j to obtain the sky brightness temperature difference ΔT_i. In addition, the correction factors for beam efficiency and blackbody function also apply to radio sources found within the RING fields. A source of flux density S in the center of the main beam of a RING field (with an attenuation factor for telescope gain at the zenith angle of the RING of 0.935 $\pm$ 0.013) produces a temperature difference $\Delta T = gS$, where $g = 0.251 \pm 0.014$ K Jy^{-1} is the effective gain of a FLUX measurement.

TABLE 1

SUMMARY OF SYSTEM CALIBRATION

Observing Session	$T_{\rm HCAL}$ (K)	$T_{\rm LCAL}$ (K)
1986 Dec 01–1987 Apr 23	23.10 $\pm$ 0.41	0.912 $\pm$ 0.016
1988 Aug 30–1989 Jan 3	21.47 $\pm$ 0.43	0.848 $\pm$ 0.017
1989 Jan 18–1989 Mar 17	26.16 $\pm$ 0.14	1.033 $\pm$ 0.006

Other parameters: HCAL/LCAL = 25.33 $\pm$ 0.06; $\eta_A = 0.280 \pm 0.009$; $\eta_B = 0.47 \pm 0.02$; $\xi = 7.99 \pm 0.26$ K Jy^{-1}; $\kappa = 2.22 \pm 0.10$; $g = 0.251 \pm 0.014$ K Jy^{-1}.

2.2. *Data*

The observations were carried out beginning in 1986 November and completed in 1989 March. A total of 173 days on the telescope were used to obtain 554 hr of integration time. The data were edited, based on weather, telescope performance monitoring, and noise analysis to produce a final data set consisting of 49898 FLUX measurements in 4195 12 minute scans—an average of 44 scans per field. A breakdown of actual telescope and final integration times is presented in Table 2.

2.2.1. *Noise and Editing*

The maser receiver itself, the associated electronics, the waveguides and feed horns, the column of atmosphere in the view of the antenna, stray radiation from the ground, and the cosmic microwave background all contribute to the signal that is measured by our system. We can equate the power detected from these sources to the power received from a thermal bath at the equivalent *system temperature* $T_{\rm sys}$ in which the entire antenna is immersed. The relation for the noise in our double switching is

$$\sigma = \frac{2T_{\rm sys}}{\sqrt{\tau \Delta \nu}}, \qquad (2)$$

where the factor of 2 is from the Dicke switching. This was used to deduce $T_{\rm sys}$ from the variance measured in integrations of length τ at the detector output. On the other hand, the power received from the atmosphere varies with time and position in the sky, which also causes the detected output to vary. Atmospheric noise and receiver gain variations are not Gaussian, but if enough samples are taken over a long enough time period, typically a few hours, then the statistics are approximately Gaussian. But while the receiver noise will integrate down with time and bandwidth as given by the factor in equation (2), atmospheric noise will in general have structures that persist over the length of a FLUX measurement. Even though these variations are much smaller than the typical 10–15 K column of water vapor that contributes to the $T_{\rm sys}$ for any single FLUX measurement, they will add a large fluctuation level that will be apparent over longer time scales. For example, 1 mK rms variations that persist, which produce rms Δt of 0.45 mK in the FLUX measurements, would from equation (2) be equivalent to an increase in system temperature of 28.5 K. We use the *noise temperature* $T_{\rm noise}$ to denote the equivalent temperature deduced from the variance between the FLUX measurements, which includes contributions from both the system temperature $T_{\rm sys}$ and external sky signals.

TABLE 2

BREAKDOWN OF RING OBSERVING TIME

Observing Season	Telescope Time (days)	Useful Time (days)	Integration Time[a] (hr)
1986 Dec 8–31	24	21	131
1987 Jan 1–May 11	40	21	94
1987 Nov–1988 May[b]	(>100)	0	0
1988 Nov 26–1989 Jan 11	47	16	65
1989 Jan 12–1989 Mar 17	62	43	264
Total	173	101	554

[a] Integration time after preliminary editing (see text).

[b] Season 1987 November–1988 May lost (see text). Time not included in total.

The data set was first edited by removing the points taken during periods when conditions were known to be unfavorable due to excessive clouds, high winds, ice on the dish surface, or equipment malfunction. Individual 40 s FLUX measurements Δt were then excised if the associated error was larger than 1.33 mK, a cutoff corresponding to $T_{\rm noise} > 84$ K, twice that for an assumed system temperature of 42 K. Next, a variance was calculated for 2 hr blocks of data, typically involving six different fields but providing a sufficient number of samples to define a variance, and the data in this period were noted as suspect if the noise temperature associated with the variance was higher than 84 K. The interfield variations (approximately 0.15 mK peak, 0.05 mK rms) should not significantly bias the flagging process, being a small fraction of the 1.33 mK cutoff noise level.

If a 2 hr section was deemed suspect under the criteria outlined above, the individual FLUX measurements in each field scan comprising the block in question were examined, and those with internal standard deviations greater than 1.33 mK were noted. If this increased noise was due to a single FLUX measurement with a value more than 1.99 mK (equivalent to 3 times $T_{\rm sys} = 42$ K) away from the scan mean, then the offending point was removed. If more than a single FLUX was suspect, then the entire scan was discarded. This is one of only two points in the selection procedure where data were rejected based on the deviation from a mean value. Use of a sample mean (in this case the average for the scan) ensures that no bias toward a particular value is generated, while the removal of only single measurements or entire scans prevents improper "weeding" out of measurements on the Gaussian noise tail and underestimation of the noise level. If none of the constituent scans had abnormal noise levels, then all data were left in under the assumption that the scatter was due to the differences between the mean values of the scans. If more than a couple of scans in a questionable 2 hr block had large errors, then all scans in that block were thrown out. Great care was taken to avoid the introduction of bias in the data through the editing process, and the use of the internal scatter as the primary standard for rejection and minimization of the use of mean values was chosen with this in mind.

With reference to Table 2, the "integration" time of 554 hr refers to data that have passed all the above tests. Approximately 42% of the telescope time was deemed as "not useful" due to poor weather, equipment failure, or other causes determined by real-time monitoring of the system. A further 45% of the original data was discarded in the noise-based editing procedure. The resulting efficiency of 13% is the same as that in the NCP experiment, even though slightly different rejection criteria were used. The automatic editing procedure used in the NCP survey was not implemented during reduction of the RING due to the small number of FLUX measurements (~ 10) comprising a typical scan. This is in contrast to the previous observations where the ~ 60 data points per scan provided ample statistics for identification of bad measurements. Measurements taken more than 6.6 minutes from transit, where the angle between the beam switching in fixed zenith angle and the circle of constant declination is greater than 1°.65, were also removed, leaving 43,977 FLUX points (488.6 hr integration, 5.1 yr per field) in 4195 scans, bringing our efficiency to 12%.

2.2.2. *Tests of Data Quality*

There are various tests we can perform to assess data quality and robustness of the set as a whole. Monitoring of the equivalent noise and variance of the individual FLUXes, scans, 2 hr

TABLE 3

TIME SCALE OF NOISE

Time Scale	σ (mK)	T_{noise} (K)
40^s FLUX point	0.65 ± 0.09	41.1 ± 5.7
12^m scan	1.05 ± 0.28	66.4 ± 16.4
>2 hr blocks	1.08 ± 0.04	67.8 ± 2.2

blocks, and the data that comprise the field measurements provides information both on possible problems in the system and on the effect of the noise contribution from the receiver and atmosphere. The results from this exercise are summarized in Table 3. We find a 0.40 mK increase in the rms noise from time scales of 40 s to 12 minutes, and a further increase of 0.03 mK from 12 minutes to the entire data set; the total increase of 0.43 mK in the FLUX measurements corresponds to 0.95 mK on-sky, equivalent to $\Delta T_{noise} = 27$ K. Since the noise is dominated by water vapor emission from the atmosphere and we estimate the path length at the elevation of the RING to contribute 13 K (a 8 K/air-mass column at 1.6 air masses), we should not be surprised to find ~ 1 mK variations on these spatial and temporal scales. Such atmospheric structures will average out as long as they do not persist on time scales of days. Indeed, the fact that the noise level ceases to increase for periods longer than 2 hr demonstrates that things stabilize over this interval. If coherent atmospheric patterns remain on longer time scales, then they should manifest themselves in the form of a bias in the mean level of the RING field fluxes, which are each tracked across the same small region of the sky. Fluctuations that are celestial in origin should average to zero on account of the nearly interlocked main and reference beam geometry adopted for this experiment, while any significant residual could be attributed to long-term cloud patterns or other systematic problems. We will see below that there is no evidence for a residual bias of this form in our data set.

The 43,977 FLUXes are plotted in histogram form in Figure 2 along with the best-fit Gaussian ($\sigma = 2.45$ mK) distribution function to the unweighted data. These numbers have been corrected to the on-sky temperature. Using the Kolmogorov-Smirnov (KS) test of this distribution against a Gaussian, we find a probability of 61%, and thus there is no indication of systematic or non-Gaussian behavior in the noise characteristics when the data set is considered as a whole. If we bin the data into 2 hr intervals in Pacific Standard Time (PST) of observation, shown in Figure 3*a*, we also find no discernible deviation from zero, obtaining a χ^2 of 8.8 for 11 degrees of freedom (probability 36%) in the twelve 2 hr bins. Note that because the observing season lasts from November until April, any given field is observed over nearly 12 hr in PST (field NPR0000 covers the range 10:00–22:00 PST), and each PST bin fairly samples half of the fields. Also shown in Figure 3*b* is the scatter among the FLUX measurements in the PST bins. No significant trend is seen.

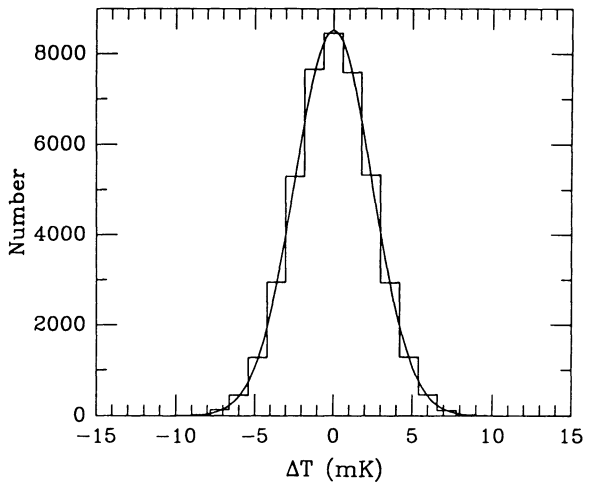

FIG. 2.—A histogram of the 43,977 calibrated FLUX measurements $\Delta T_{ij} = \kappa \Delta t_{ij}$. The superposed curve is the number expected if drawn from a normal $N(0, \sigma)$ distribution with $\sigma = 2.45$ mK.

2.2.3. *Weighting and the Final Edit*

To obtain the final value for each field, the mean and uncertainty of the FLUXes in a given field were computed using weights given by the FLUX errors ϵ_i^j. For field i, with FLUXes and errors $\{\Delta t_i^j, \epsilon_i^j\}, j = 1, \ldots, n_i$:

$$\Delta T_i = \frac{1}{W_i} \sum_{j=1}^{n_i} \frac{\kappa \Delta t_i^j}{(\epsilon_i^j)^2}, \tag{3a}$$

$$\sigma_i^2 = \frac{n_i}{n_i - 1} \frac{1}{W_i} \sum_{j=1}^{n_i} \frac{(\kappa \Delta t_i^j - \Delta T_i)^2}{(\epsilon_i^j)^2}, \tag{3b}$$

$$\epsilon_i^2 = \frac{1}{n_i} \sigma_i^2, \tag{3c}$$

$$W_i = \sum_{j=1}^{n_i} \frac{1}{(\epsilon_i^j)^2}, \tag{3d}$$

where $\kappa = 2.22$ is the correction factor (see above) to sky brightness temperature. We choose to use the FLUX error as a weighting parameter because the preferred statistic, the scan variance, which we have shown is a much better estimate on average of the increase in T_{noise} due to the water vapor structures in the atmosphere, is not sufficiently well determined with only the 10 FLUXes obtained on average for each scan. Although this underestimates the true noise level, the FLUX error should be stable, being made up of 80 half-second integrations, and provides a reasonable estimate of the relative noise levels in the different measurements. It is also desirable to remove the FLUX measurements that lie on the tail of the distribution (Fig. 2); we test against the mean for the field i and reject a point Δt_i^j if $|\kappa \Delta t_i^j - \Delta T_i| \geq q\sigma_i$ for cutoff parameter q. This is the second and last time where the mean value is used as a criterion for acceptance of data, and is used to remove grossly discrepant measurements caused, for example, by interference. In fact, examination of Figure 2 shows that the tail is well behaved, and no problems or systematic bias should arise from this step. We adopt the conservative value $q = 4$ and find that only six FLUXes are excluded in this step.

3. ANALYSIS

3.1. *Preliminary Statistical Analysis*

The entire data set of 49,898 FLUXes was collated into the 96 fields and analyzed. At this point, 10 FLUXes with errors greater than 2.98 mK (after correction to the on-sky brightness temperature) were discarded. Of the remainder, 43,977 lie within ± 6.6 minutes of transit. Finally, six more FLUX points were rejected as having values more than 4 σ_i away from ΔT_i, leaving us with 43,971 FLUXes from 4195 scans to generate

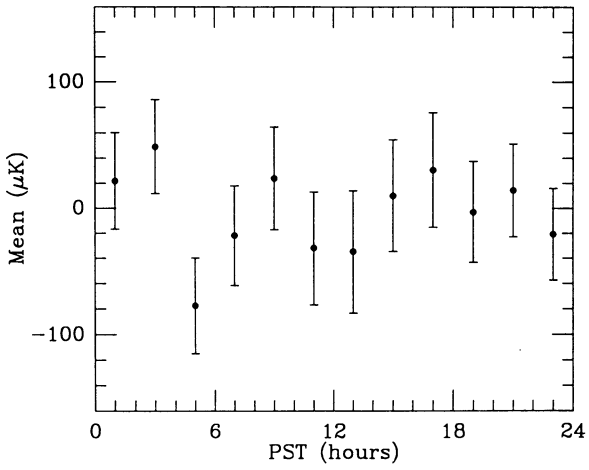

FIG. 3a

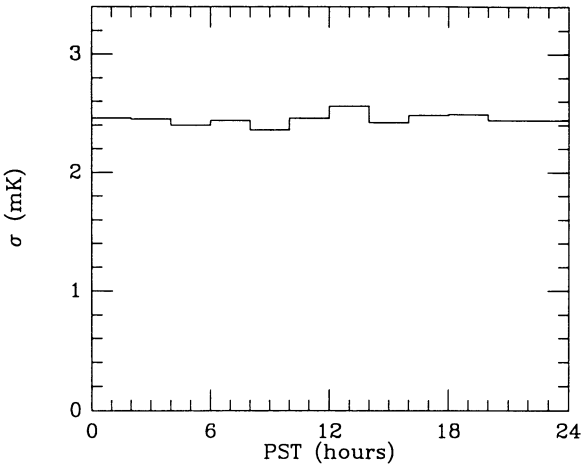

FIG. 3b

FIG. 3.—The mean (*a*) and standard deviation (*b*) for 43,977 RING data points binned into 2 hr intervals in Pacific Standard Time (PST). The error bars in (*a*) are $\pm 1\ \sigma$ standard deviation in the mean. The value of χ^2 in (*a*) is 8.8 on 11 degrees of freedom.

the set of 96 $\{\Delta T_k, \epsilon_k\}$. The results for the 96 fields are plotted in Figure 4 and tabulated in Table 4. We remind the reader that no mean or derivative has been subtracted from the data. The first thing to note is that the largest deviation from zero is 4.1 σ. The second is that those fields that show significant signal are flanked by fields with means of the opposite sign, as is expected, with our switching scheme, for real signals.

We can form the weighted mean of the 96 fields in a manner similar to that used to calculate the field values,

$$\bar{T} = \frac{1}{W} \sum_{i=1}^{96} \frac{\Delta T_i}{\epsilon_i^2}, \tag{4a}$$

$$\sigma \frac{2}{T} = \frac{1}{W}, \tag{4b}$$

$$\sigma_{\rm tot}^2 = \frac{96}{95W} \sum_{i=1}^{96} \frac{(\Delta T_i - \bar{T})^2}{\epsilon_i^2}, \tag{4c}$$

$$W = \sum_{i=1}^{96} \frac{1}{\epsilon_i^2}, \tag{4d}$$

$$\bar{\epsilon}_{\rm fld} = \frac{1}{96} \sum_{i=1}^{96} \epsilon_i . \tag{4e}$$

For the entire RING data set, we find $\bar{T} = -6.1 \pm 11.5\ \mu$K, $\sigma_{\rm tot} = 175.8\ \mu$K, and mean error $\bar{\epsilon}_{\rm fld} = 113.4 \pm 8.4\ \mu$K. We have tabulated the RING means by the epoch of observation as well as for the total data set in Table 5. The values of $\bar{T} \pm \sigma_{\bar{T}}$ were computed for the $n_{\rm tot}$ FLUX measurements within individual data intervals. The maximum likelihood estimator for the excess standard deviation $\hat{\sigma}_{\rm sky}$ was calculated in the manner described below. We find no evidence for aberrant sections of data, although the deviation of some means from zero is uncomfortably large, especially the 3.5 σ excursion of the 1987 value. This behavior is reminiscent of that exhibited in 1985 December during the NCP observations (Paper 1). The fact that the mean for the entire data set, $-6.1 \pm 11.5\ \mu$K, is consistent with zero leads us to conclude that any postulated bias mechanism may operate over time scales of several months but must average to zero over our 3.5 yr baseline. *Because the average is consistent with zero and none of our tests show any significant behavior inconsistent with the estimated noise levels, we conclude that the RING is free from significant systematic biases.*

There is an excess variance in field means above that expected from the uncertainties shown by the error bars. This is most easily shown by ignoring the correlations between measurements and assuming the ΔT_i to be independent Gaussian variables with a variance given by $\sigma_{\rm sky}^2 + \epsilon_i^2$. We find

$$\sigma_{\rm sky} \simeq \sqrt{\sigma_{\rm tot}^2 - 96\ \sigma_{\bar{T}}^2} = 134.9\ \mu{\rm K}\ . \tag{5}$$

We now use several other methods to characterize the significance of this signal in the RING data.

The Bayesian formalism of Paper 1 can also be used to place limits on the magnitude of the excess signal in the measurements, neglecting for the time being the correlation properties of any assumed random field or the actual correlations between the interlocked RING fields themselves. If $\sigma_{\rm sky}^2$ is the contribution to the variance from sources not attributable to

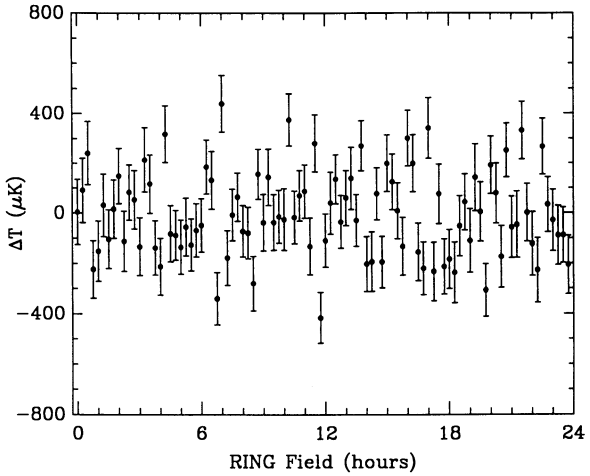

FIG. 4.—RING measurements of field values ΔT_i, corrected to on-sky temperature. The error bars are ϵ_i, the $\pm 1\ \sigma$ standard deviation in the means. A total of 43,971 individual FLUX measurements are included from within 6.6 minutes of transit.

TABLE 4

RESULTS OF RING OBSERVATIONS

Field	α (1950)	δ (1950)	ΔT_i (μK)	ϵ_i (μK)	σ_i (mK)	n_i	Field	α (1950)	δ (1950)	ΔT_i (μK)	ϵ_i (μK)	σ_i (mK)	n_i
NPR0000	235812.1	875820.5	4.7	130.0	2.42	349	NPR1200	115759.0	882303.5	-109.2	106.2	2.31	473
NPR0015	001140.7	875821.7	91.4	129.3	2.37	336	NPR1215	121453.6	882301.9	40.4	124.2	2.55	422
NPR0030	002509.6	875825.8	240.8	128.1	2.53	389	NPR1230	123147.6	882256.8	135.8	99.1	2.25	514
NPR0045	003839.1	875832.8	-223.8	114.1	2.46	464	NPR1245	124840.2	882248.1	-34.5	105.0	2.38	513
NPR0100	005209.3	875842.5	-151.2	120.0	2.35	384	NPR1300	130530.8	882236.0	60.6	110.4	2.42	479
NPR0115	010540.7	875855.0	31.5	125.0	2.39	366	NPR1315	132218.8	882220.4	139.7	125.4	2.49	395
NPR0130	011913.5	875910.3	-103.5	117.3	2.41	422	NPR1330	133903.5	882201.5	-28.9	102.2	2.28	499
NPR0145	013247.9	875928.3	16.5	116.3	2.40	425	NPR1345	135544.3	882139.4	270.6	100.9	2.30	518
NPR0200	014624.3	875948.9	148.8	111.6	2.30	425	NPR1400	141220.7	882114.3	-202.2	109.5	2.32	448
NPR0215	020002.9	880012.1	-111.8	120.5	2.49	428	NPR1415	142852.3	882046.2	-193.1	118.1	2.47	436
NPR0230	021344.0	880037.8	83.1	110.7	2.33	442	NPR1430	144518.5	882015.3	77.7	104.0	2.39	529
NPR0245	022728.0	880105.9	53.7	116.9	2.40	422	NPR1445	150139.0	881941.8	-194.5	102.7	2.36	526
NPR0300	024115.0	880136.3	-133.5	115.4	2.39	431	NPR1500	151753.4	881905.9	200.1	114.4	2.38	434
NPR0315	025505.3	880208.9	214.3	129.7	2.55	386	NPR1515	153401.4	881827.8	125.5	111.8	2.33	435
NPR0330	030859.3	880243.7	116.9	117.3	2.46	439	NPR1530	155002.8	881747.7	9.6	111.6	2.47	488
NPR0345	032257.3	880320.4	-138.3	108.3	2.31	457	NPR1545	160557.5	881705.8	-131.9	114.9	2.55	492
NPR0400	033659.4	880359.1	-212.9	112.7	2.48	486	NPR1600	162145.1	881622.3	301.1	111.3	2.44	479
NPR0415	035106.0	880439.4	317.6	113.5	2.37	435	NPR1615	163725.8	881537.5	199.8	114.8	2.39	432
NPR0430	040517.3	880521.3	-81.9	111.6	2.47	489	NPR1630	165259.4	881451.4	-154.7	114.8	2.48	468
NPR0445	041933.7	880604.7	-88.1	99.4	2.25	514	NPR1645	170825.9	881404.5	-220.2	104.7	2.33	496
NPR0500	043355.3	880649.3	-135.1	108.3	2.45	510	NPR1700	172345.4	881316.8	341.5	121.3	2.47	413
NPR0515	044822.4	880735.1	-54.8	114.9	2.40	436	NPR1715	173857.9	881228.6	-232.7	115.9	2.30	395
NPR0530	050255.3	880821.8	-126.2	103.5	2.38	529	NPR1730	175403.5	881140.2	76.7	119.2	2.37	396
NPR0545	051734.2	880909.2	-68.3	106.0	2.44	528	NPR1745	180902.4	881051.7	-213.0	109.5	2.38	473
NPR0600	053219.3	880957.2	-48.2	106.1	2.47	544	NPR1800	182354.7	881003.3	-183.4	117.7	2.45	434
NPR0615	054710.7	881045.5	185.5	109.0	2.37	474	NPR1815	183840.6	880915.2	-236.6	120.5	2.43	407
NPR0630	060208.8	881134.0	132.3	116.2	2.54	477	NPR1830	185320.2	880827.7	-51.3	119.8	2.40	400
NPR0645	061713.5	881222.5	-339.9	103.9	2.46	559	NPR1845	190753.9	880740.9	44.1	112.5	2.38	447
NPR0700	063225.2	881310.7	439.2	112.6	2.50	494	NPR1900	192221.7	880655.1	-109.9	127.0	2.62	426
NPR0715	064743.8	881358.5	-178.3	109.4	2.44	497	NPR1915	193644.0	880610.3	143.2	134.4	2.55	360
NPR0730	070309.4	881445.5	-7.0	102.5	2.45	571	NPR1930	195101.0	880526.7	5.7	118.4	2.51	449
NPR0745	071842.1	881531.7	64.4	96.3	2.42	630	NPR1945	200513.0	880444.6	-306.6	104.4	2.31	491
NPR0800	073421.9	881616.7	-71.8	102.0	2.37	538	NPR2000	201920.2	880404.1	192.2	116.3	2.46	446
NPR0815	075008.7	881700.4	-79.2	102.6	2.36	527	NPR2015	203322.8	880325.2	79.9	120.9	2.37	385
NPR0830	080602.4	881742.5	-279.9	108.0	2.45	515	NPR2030	204721.3	880248.2	-173.9	123.1	2.57	436
NPR0845	082203.0	881822.9	156.2	100.7	2.40	567	NPR2045	210115.8	880213.2	252.1	108.4	2.44	505
NPR0900	083810.2	881901.2	-37.7	112.0	2.48	492	NPR2100	211506.6	880140.3	-56.3	122.6	2.39	381
NPR0915	085423.8	881937.4	144.0	113.9	2.38	435	NPR2115	212854.0	880109.6	-45.6	132.2	2.58	381
NPR0930	091043.6	882011.2	-36.9	110.5	2.38	463	NPR2130	214238.3	880041.2	332.4	115.3	2.30	397
NPR0945	092709.1	882042.4	-14.0	105.1	2.46	546	NPR2145	215619.8	880015.2	2.1	115.3	2.40	433
NPR1000	094340.0	882110.9	-24.9	122.9	2.51	418	NPR2200	220958.7	875951.7	-122.5	127.0	2.40	358
NPR1015	100015.8	882136.4	374.9	104.4	2.23	456	NPR2215	222335.3	875930.8	-227.1	128.1	2.59	409
NPR1030	101656.1	882158.9	-17.0	105.1	2.37	509	NPR2230	223710.0	875912.4	267.3	112.7	2.38	447
NPR1045	103340.3	882218.2	70.1	100.8	2.40	567	NPR2245	225043.0	875856.8	33.7	109.8	2.32	446
NPR1100	105027.9	882234.2	87.0	107.4	2.30	461	NPR2300	230414.5	875843.9	-28.5	122.4	2.31	357
NPR1115	110718.2	882246.8	-132.1	112.9	2.45	470	NPR2315	231744.9	875833.8	-88.5	117.8	2.37	405
NPR1130	112410.6	882255.9	280.4	114.5	2.56	499	NPR2330	233114.4	875826.6	-87.9	110.4	2.26	418
NPR1145	114104.5	882301.5	-416.0	100.5	2.38	561	NPR2345	234443.4	875822.1	-206.3	115.9	2.43	438

the measurement errors, then the likelihood function for the parameter σ_{sky} with the distribution mean $\mu = 0$ is

$$L(\sigma_{sky}) = \prod_{i=1}^{96} \frac{1}{\sqrt{2\pi(\epsilon_i^2 + \sigma_{sky}^2)}} \exp\left[-\frac{\Delta T_i^2}{2(\epsilon_i^2 + \sigma_{sky}^2)}\right]. \quad (6)$$

The likelihood function for the RING data is plotted in Figure 5. The value of σ_{sky} at the maximum likelihood is denoted $\hat{\sigma}_{sky}$, the maximum likelihood method (MLM) estimator of the signal rms listed in Table 5. For the entire RING data set, this value is $\hat{\sigma}_{sky} = 133.4$ μK. The likelihood function is detached from the origin and very narrow, with a width given by

$$\sigma_{\hat{\sigma}_{sky}} \sim \frac{\hat{\sigma}_{sky}}{\sqrt{192}}, \quad (7)$$

and because of this we can dispense with worries about the choice of the Bayesian prior over the range in σ_{sky} for which L contributes. We can integrate this L over the range of σ_{sky} containing its maximum values to obtain the desired highest probability density (HPD) credible intervals (the Bayesian equivalent of confidence limits—see Berger 1985; Myers 1990) in σ_{sky}:

$$\begin{aligned} 103 < \sigma_{sky} < 168\ \mu\text{K} \quad (95\%) \\ 85 < \sigma_{sky} < 194\ \mu\text{K} \quad (99.87\%)\,. \end{aligned} \qquad \hat{\sigma}_{sky} = 133\ \mu\text{K} \quad (8)$$

These detections are well above the NCP program 95% upper limit of 58 μK and marginally inconsistent with the NCP 99.87% upper limit of 127 μK, assuming independent uncorrelated Gaussian fluctuations. In this and all forthcoming analyses, *no mean is subtracted from the data.* Subtraction of the sample mean $\bar{T} = -6$ μK in computing L would change these limits by less than 1 μK. The value of the likelihood for $\sigma_{sky} = 0$ is 3×10^{-12} with respect to the maximum at

TABLE 5

RING RESULTS BY EPOCH

Observing Season	$\bar{T} \pm \sigma_{\bar{T}}$ (μK)	$\hat{\sigma}_{sky}$ (μK)	n_{tot}
1986 Dec 8–29	22.0 ± 23.5	174.3	10375
1987 Jan 1–Apr 22	−93.9 ± 26.9	188.4	7441
1988 Nov 26–1989 Jan 3	−50.9 ± 34.3	270.6	5204
1989 Jan 12–Mar 17	14.9 ± 16.5	148.8	20951
All data	−6.1 ± 11.5	133.4	43971

$\hat{\sigma}_{sky}$. The extreme significance of this value, however, is due mostly to the narrowness of the function. We quote both 95% and 99.87% (equivalent to 3 σ for a Gaussian distribution) for comparison with other limits but prefer the conservative use of the 99.87% figures. A threshold of 3 σ or higher is standard in experimental physics, and we feel there is no good reason to relax this when applying statistical methods to observations of the microwave background radiation.

We can also test the distribution of RING field values against that expected for the Gaussian errors alone. We divide the field means by their associated errors

$$\chi_i = \frac{\Delta T_i}{(\epsilon_i^2 + \sigma_{sky}^2)^{1/2}} \tag{9}$$

and then construct the cumulative distribution function $S(\chi)$ of the n values $\{\chi_i\}$ ranked in ascending order

$$S(\chi) = \begin{cases} 0 & \chi < \chi_1 \\ \dfrac{i}{n} & \chi_i \le \chi < \chi_{i+1} \\ 1 & \chi \ge \chi_n \end{cases}, \tag{10}$$

which we will compare to the model cumulative distribution function $F(\chi)$. For Gaussian errors and signal, the parent distribution of χ is a normal $N(0, 1)$, and the model distribution F is

$$F(\chi) = \frac{1}{2} + \frac{1}{2}\,\mathrm{erf}\left(\frac{\chi}{\sqrt{2}}\right). \tag{11}$$

For the test, we use the well-known nonparametric Kolmogorov-Smirnov test (see Kendall & Stuart 1979, §§ 30.49–30.55). This test uses the statistic D_n, which measures the maximum deviation of the steplike function S from the theoretical distribution function F for a sample of n points. If we wish to test against the hypothesis of no signal, then we set $\sigma_{sky} = 0$ and compute D_n. In Figure 6*a*, both S and F are shown for $\sigma_{sky} = 0$, which yields a probability $P(> D_n) = 0.064$. A histogram of the χ-values and the test Gaussian is shown in Figure 6*b*. If we increase the excess variance to $\sigma_{sky} = 133$ μK, we find a probability of 0.90 for the distribution function shown in Figures 6*c* and 6*d*. The significance of the KS test result of 6.4% against a null signal is lower than one might have expected given the extremely strong rejection of zero by the likelihood or Bayesian method above. However, this is mostly due to the weighting of the standard tests toward the tail of the distribution. Because a parametric test such as the Bayesian HPD method is designed to extract the maximum amount of information available in the data about the parameter under consideration, it is more powerful than a general nonparametric method such as the KS test. The failure of the KS test to produce a strong result should, however, warn us that our detection of excess variance is likely to be based on a few large values on the tail of the distribution.

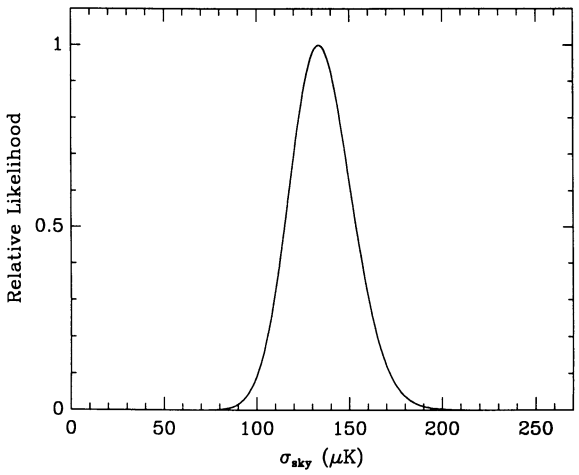

FIG. 5.—Likelihood function for σ_{sky} from the RING data, normalized to the maximum at $\hat{\sigma}_{sky} = 133.4$ μK. The relative likelihood at $\sigma_{sky} = 0$ is 2.8×10^{-12}.

3.2. *The Source of Excess Variance*

We have shown that there exists in the RING data set an excess of variance over that expected given the errors. It is necessary to identify the specific RING fields in which there are suspected sources, microwave background or otherwise. Before proceeding further, we must demonstrate that the origin of this signal is on the sky, rather than in the instrument or the atmosphere or due to an underestimate of the errors. The fact that the RING fields interlock makes such a determination possible. Once again, more than one analytical technique will be used.

The interlocked sampling geometry of the RING experiment was chosen so that the reconstruction would be possible on a field-by-field basis by deconvolution of the switching pattern. The closure of the RING compensates for the loss of the gradient information in the individual double-differences, and the mean level remains as the only undetermined parameter. This also means that there is information on the correlation function of the CMBR on scales up to the RING diameter, and this should be taken into account in our Bayesian analysis of variance. It should be remembered that the RING fields do not interlock exactly, as there is a difference of 14′.4 between the azimuth switching reference field position at target field transit and the adjacent field main beam location on the circle of constant declination. In addition, the two beams are not perfectly symmetric, and there are irregularities in the OVRO primary beam below the 20% power level. The import of these nonuniformities will be discussed more fully in relation to the point source contribution. There is no significant effect on the results expected for a diffuse signal such as the microwave background anisotropy.

3.2.1. *Correlation Analysis*

One approach to analysis of the RING data is to evaluate the correlation between the measurements ΔT_i. We can define the RING correlation function

$$C_k = \tfrac{1}{96} \sum_{i=1}^{96} \Delta T_i \Delta T_{i+k}\,. \tag{12}$$

The results for the RING are shown in Figure 7. Beyond the

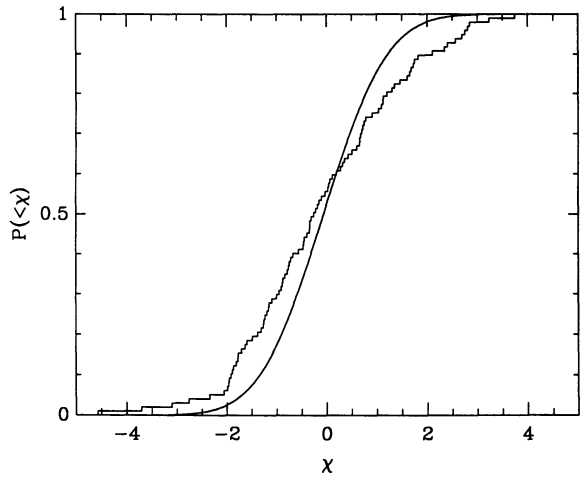

FIG. 6a

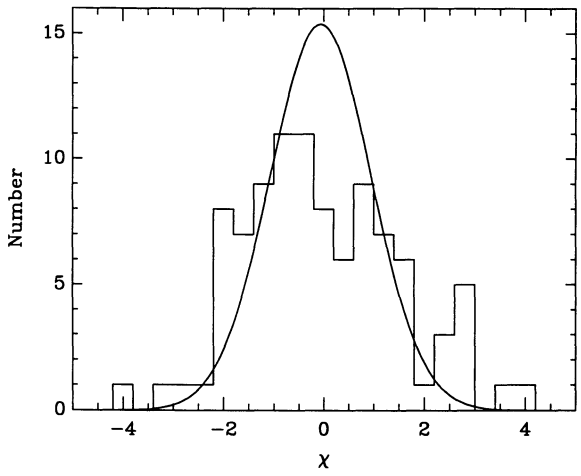

FIG. 6b

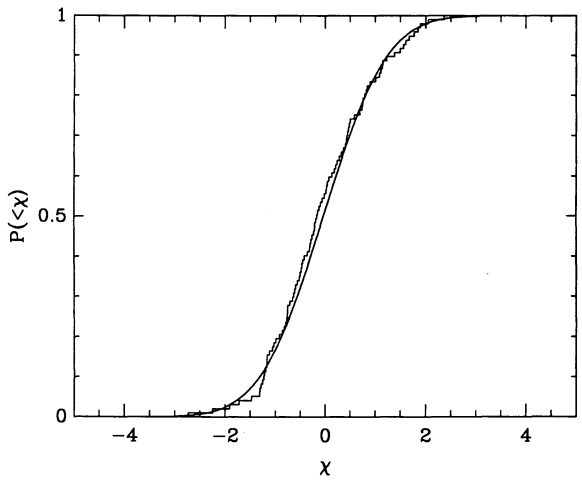

FIG. 6c

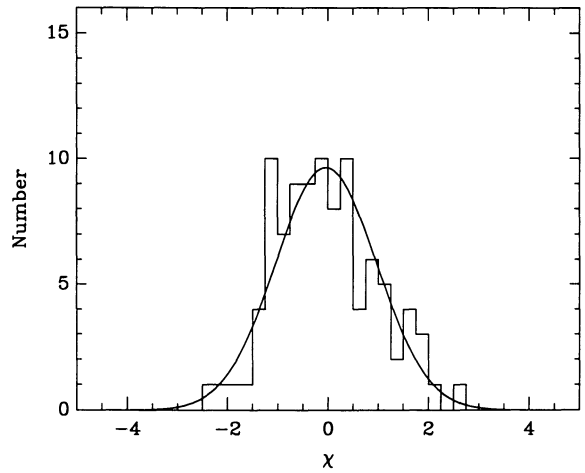

FIG. 6d

FIG. 6.—The distribution of RING field means ΔT_i. The cumulative distribution function for $\chi_i = \Delta T_i/\epsilon_i$ is shown in (*a*) with the normal $N(0, 1)$ curve superposed. The KS probability of a deviation this large or larger is 6.4%. Panel (*b*) is the histogram of the χ_i-values from (*a*). The solid curve is the number expected for a normal $N(0, 1)$ distribution. The cumulative distribution function of $\chi_i = \Delta T_i/(\epsilon_i^2 + \sigma_{sky}^2)^{1/2}$ for $\sigma_{sky} = 133$ μK is shown in (*c*), with the normal $N(0, 1)$ curve. The KS probability of a deviation this large or larger is 90%. Panel (*d*) is the histogram of the χ-values from (*c*), along with the expected counts for a $N(0, 1)$ distribution.

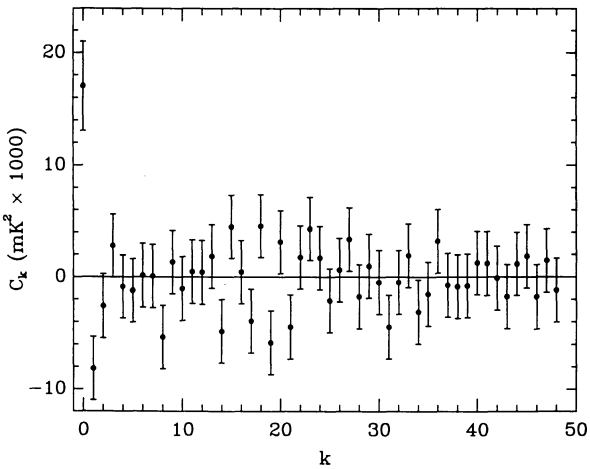

FIG. 7.—Correlation function for RING data. Error bars are derived by propagation of errors using the ϵ_i. The significance of C_0 is 4.3 σ, while that of C_1 is 2.9 σ.

first two components C_0 and C_1, no significant correlations are found in the data. In addition to any true correlations on-sky, there are correlations induced by the beam switching. Using the expression for RING measurements ΔT_i given in equation (1), and adding the *independent* Gaussian measurement errors, we find for *independent* fields T_j,

$$\langle C_0 \rangle = \tfrac{3}{2}(\langle T^2 \rangle - \langle T \rangle^2) + \tfrac{1}{96} \sum_{i=1}^{96} \epsilon_i^2 ,$$
$$\langle C_1 \rangle = -(\langle T^2 \rangle - \langle T \rangle^2) . \tag{13}$$

The expected ratio of the two correlation functions after subtraction of the noise term from C_0 is thus

$$\frac{\langle C_0 \rangle}{\langle C_1 \rangle} = -\frac{3}{2} . \tag{14}$$

For the RING data we find

$$C_0 = 17.04 \times 10^{-3} \pm 3.97 \times 10^{-3} \text{ mK}^2 ,$$
$$C_1 = -8.16 \times 10^{-3} \pm 2.84 \times 10^{-3} \text{ mK}^2 , \tag{15}$$

and thus

$$\frac{C_0}{C_1} = -2.09 \pm 0.88 \,. \tag{16}$$

This is consistent with equation (14) given the uncertainty and supports the conclusion that the excess signal in C_0 is due to on-sky signal as opposed to uncorrelated noise. Noise from the instrument or the atmosphere would not be expected to produce a negative C_1, thus our variance is likely to be celestial in origin. A higher signal-to-noise ratio is needed, however, to extract further information from the correlation analysis.

3.2.2. *Matched Filtering*

The first thing we do to locate those fields in which there are significant signals is to convolve the RING with the "matched filter" provided by the switching pattern itself,

$$f_i = \tfrac{2}{3}(\delta_i - \tfrac{1}{2}\delta_{i-1} - \tfrac{1}{2}\delta_{i+1}) \,, \tag{17}$$

where $\delta_i \equiv \delta_{i0}$ is the Kronecker δ-function. The normalization in equation (17) is such that the strength of an isolated source will be given by the filtered value. It is easy to show, by application of the Cauchy inequality, that this process yields the maximum signal-to-noise ratio for the detection of signals in noise provided that the noise in different RING fields is uncorrelated and of approximately the same level. The result of this method for the RING is shown in Figure 8. There are 10 fields with filtered levels above the 3 σ level: NPR0415, NPR0700, NPR1015, NPR1130, NPR1345, and NPR1700 and the negative fields NPR0645, NPR1145, NPR1715, and NPR1945. We can reasonably associate the negative fields as the result of positive signal in adjacent beams, except for NPR1945 (a positive source in NPR2000 would be expected to have a negative sidelobe in NPR2015, which is not seen). These seven fields are the prime candidates for real sources, microwave background or otherwise. Our statistical tests may show the presence of anisotropy, but only in these fields is it reasonable to pursue identification based on the RING data alone. If all seven fields and their adjacent "reference" fields are removed from the RING, then in the 75 remaining fields we are left with the HPD limits and MLM estimate

$$\begin{aligned} 38 < \sigma_{\rm sky} < 125 \ \mu{\rm K} \quad (95\%) \\ \sigma_{\rm sky} < 146 \ \mu{\rm K} \quad (99.87\%) \,. \end{aligned} \qquad \hat{\sigma}_{\rm sky} = 83 \ \mu{\rm K} \tag{18}$$

By removal of these fields, we have eliminated the lower limit at the 3 σ equivalent level.

3.2.3. *Deconvolution and Reconstruction*

Although it is possible to solve directly the system of equations (1) to within an overall mean value for the individual field values $\{T_i\}$ given the RING measurements $\{\Delta T_i\}$, the presence of measurement errors makes this solution useless as far as reconstruction of the actual on-sky temperatures. The double-differencing used in these observations acts as a high-pass filter on the true sky temperature distribution, and in a direct inversion the noise will enter as spurious low spatial frequency artifacts. We have tested various filtering and constrained Bayesian methods on the RING data, but the low signal-to-noise ratio in the data set prevents much useful information from being gained through this method.

There are other options for deconvolution of the signal from the noise. Deconvolution algorithms popular in astronomy, such as CLEAN and the maximum entropy method (MEM),

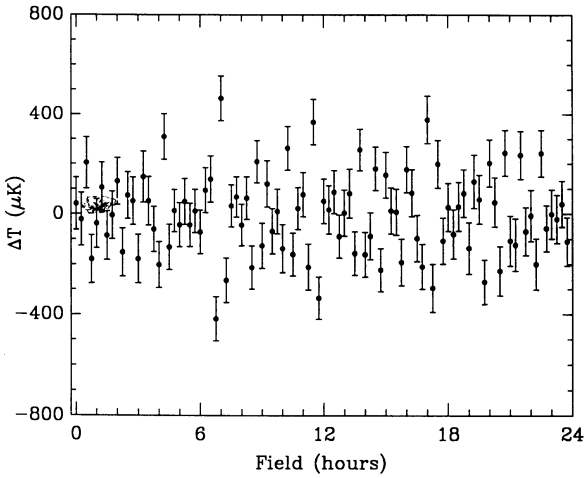

FIG. 8.—Results of matched filtering of RING fields. The kernel used is given in eq. (17), for approximately equal field errors ϵ_i. The error bars are the ± 1 σ standard deviation in the filtered values.

can be used on the RING data also. The CLEAN method (see Cornwell 1985) iteratively deconvolves the "dirty" image by locating the most extreme value in the data and adding some fraction of it as a δ-function to the "clean" image that is initially zero, and subtracting the corresponding δ-function convolved with the point-spread function from the residual "dirty" image. We have implemented a simple version of this algorithm on the RING, and find that while it deconvolves the strong isolated fields such as NPR0700 with results similar to the matched filtering, it also suffers from the high noise level in the RING data.

The maximum entropy method, extensively applied to image processing and data analysis in a variety of applications such as radio astronomical interferometry and medical imaging (Gull & Skilling 1984; Skilling 1989; Gull 1989), is a Bayesian method. We have produced a MEM image of the RING using the program MEMSYS-3.[2] The MEM algorithm ensures the positivity of the reconstructed image, although reconstruction of images with both positive and negative elements can be effected by solving simultaneously for two positive images and expressing the final map as the difference between the two. Unfortunately, the low signal-to-noise ratio of the RING data adversely affects the MEM reconstruction of isolated point sources, underestimating the strength of these objects. The constraints given by the data are unable to overcome the maximum entropy condition, which tends to smooth out the reconstruction. In this case, the matched filtering gives the best estimate of the source strength. To use the MEM on the RING data, we have made three separate reconstructions: one allowing only positive sources, one allowing only negative sources (by switching the sign of the data), and one allowing both positive and negative sources (by solving for the difference of two positive images). The results of the positive and the positive/negative solutions are shown in Figure 9, along with the MEM (Bayesian) estimated error bars.

In the MEM positive-only reconstruction (Fig. 9*a*) we find four fields (NPR0415, NPR0700, NPR1130, NPR1700) with values of 3 σ or more. In the negative-only MEM solution, two fields (NPR0645, NPR1145) are found at 3 σ as sidelobes of

[2] S. F. Gull & J. Skilling, Maximum Entropy Data Consultants Ltd., Royston, England.

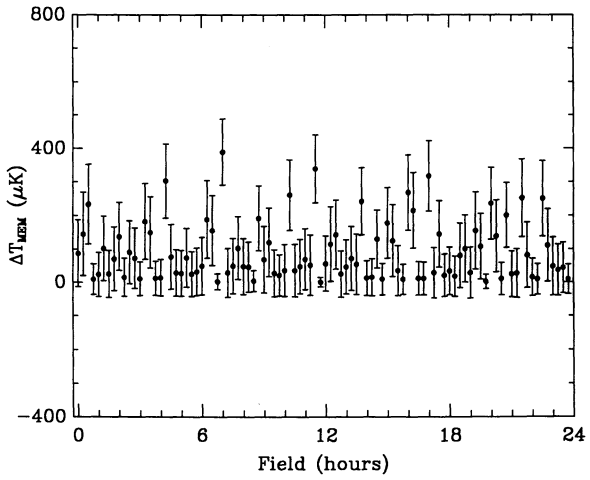

FIG. 9a

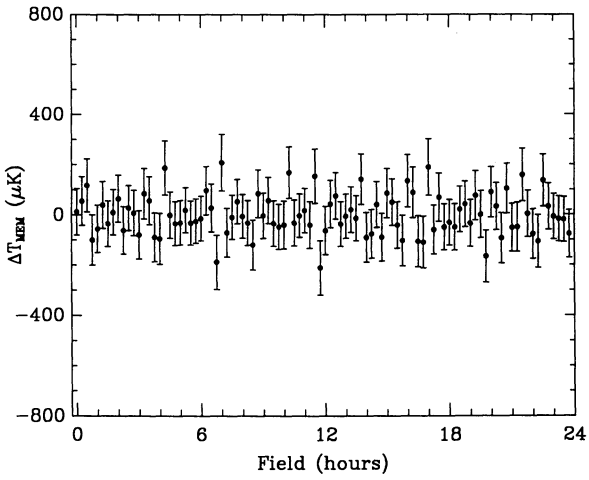

FIG. 9b

FIG. 9.—MEM reconstruction of RING sky distribution with allowance for positive intensities only (*a*) and both positive and negative temperatures (*b*). The intensities determined for the signal are biased significantly toward zero, as can be seen by comparison with the matched filtering results.

positive sources. The negative field NRP 1945 is found at only the 2.5 σ level. No fields of 3 σ or greater are found when both positive and negative solutions are allowed (Fig. 9*b*). The latter image appears to be very similar to the RING data itself, with some of the noise signal removed. More observations to obtain a higher signal-to-noise ratio would allow a much better reconstruction of the RING fields.

4. IDENTIFICATION OF SOURCES

Given the strong evidence from three different analytical techniques that the excess variance in the RING data is caused by real on-sky signals rather than instrumental artifacts or underestimation of errors, we now turn to the problem of identification of the signal in the individual fields and estimation of the contribution from known foreground objects. We are concerned with two types of contaminating sources, discrete sources of angular size much smaller than our 1.8 FWHM beam and diffuse sources of size comparable to and larger than our beam. Galactic synchrotron, free-free, and dust emission are possible diffuse foregrounds. Estimates of the levels expected for our 20 GHz measurements lead us to believe that it is unlikely that they are responsible for a significant fraction of the observed signal, although more will be said about this later. On the other hand, the discrete foreground due to extragalactic radio sources is known to be a problem at these frequencies. The NCP observations detected a 200 μK signal in one out of eight fields from a known radio source, and simple extrapolation would lead us to expect contamination of the RING experiment by around 3–12 such objects. In the RING data, we find four fields with signals of more than 3 σ away from zero: NPR0700, NPR1015 (positive), and NPR0645, NPR1145 (negative). By way of comparison, there is a 12% chance of at least one 3 σ or greater deviation expected from noise alone in the set of 96 points.

The properties and evolution of radio galaxies and quasars have been extensively studied, especially at frequencies 5 GHz and lower (see Condon 1988 for a review and references). The spectra of these sources are well explained by the superposition of synchrotron emission regions of differing optical depths. We assume a spectrum

$$S_\nu = S_{\nu_0}\left(\frac{\nu}{\nu_0}\right)^\alpha, \tag{19}$$

where α is the spectral index. So-called steep spectrum sources typically have $\alpha \sim -0.7$ between 1.4 and 5 GHz, the best-studied frequencies for flux densities below 1 Jy. For sources selected from flux-limited catalogs at 5 GHz, around 50% have flat spectra with $\alpha > -0.5$ between 1.4 and 5 GHz at flux densities below the milli-Jansky level which interests us here (Kellermann & Wall 1987; Fomalont et al. 1991). At 5 GHz, the flat spectrum sources have a wide distribution centered on $\alpha \sim 0.0$. Unfortunately, not much is known about the spectral index properties of faint radio sources selected at 20 GHz.

4.1. *Radio Source Counts*

Calculations of the contribution of discrete radio sources to microwave background anisotropy experiments have been made by Danese, De Zotti, & Mandolesi (1983) and Franceschini et al. (1989). Their results indicate that for the Owens Valley experiments, confusion can be expected at the level of 37 μK (1.3×10^{-5} in $\Delta T/T$) for the contribution to the field rms. Their different models give variations of 20% in this value. However, as noted by the authors, the distribution is skewed positive with a long tail, and use of the variance will underestimate the true level of contamination. In addition, they assume in their calculations of the variance that the experiments are limited by the confusion noise itself, unlike our case where we are limited by instrumental noise. Besides underestimation of the rms signal, these analyses ignore the inherently non-Gaussian nature of the source distribution. The differential source counts are assumed to follow a power-law form over the range of relevant flux densities

$$\frac{dN}{dS} = KS^{-\gamma} \tag{20}$$

for flux density S in janskys. For these distributions (and $\gamma > 2$) the expected rms value diverges, and some cutoff must be imposed to obtain finite limits. There are several methods that can be used to determine the statistical level of the contamination in the RING, or to use the RING to place limits on source counts at 20 GHz. In this paper we will only present some simple estimates, and a more thorough treatment will be given in a separate paper.

An estimate of the expected variance of measurements can be obtained by integration of equation (20) over a Gaussian

beam, and assuming a Poisson distribution of sources (Condon 1974),

$$\sigma^2 = 1.5 \frac{K\Omega_B}{(\gamma - 1)(3 - \gamma)} D_{\max}^{3-\gamma}, \quad (21)$$

where $\Omega_B = 3.2 \times 10^{-7}$ sr is the Gaussian main beam area, and the multiplicative factor 1.5 is from the linked three-beam switching in the RING. For power-law slopes of $\gamma < 3$, the expected rms value diverges with the upper cutoff $D_{\max}$. Furthermore, note that one-half of the contribution to the σ from equation (21) will come from sources of $D > 2^{-2/(3-\gamma)} D_{\max}$.

We are interested in sources of flux density less than 2 mJy at 20 GHz. The best estimate of faint source counts at 5 GHz at sub-millijansky flux densities is obtained from VLA surveys (Fomalont et al. 1988, 1991). They estimate the differential number-flux count to be

$$\frac{dN}{dS} = (27.4 \pm 5.5) S^{-2.18 \pm 0.19} \text{ Jy}^{-1} \text{ sr}^{-1} \quad (22)$$

in the flux density range 10 μJy–1 mJy. Using the maximum field deviation in the RING for the upper cutoff, $D_{\max} = 1.75$ mJy, will give us an estimate of the rms due to sources in the flux range seen in the RING data. For the OVRO sensitivity (0.251 K Jy^{-1}) and the above counts ($K = 27.4$, $\gamma = 2.18$) we obtain an expected RING rms value of $\sigma = 69$ μK, one-half of which will come from sources of $D > 0.18 D_{\max}$, which corresponds to $D > 79$ μK. This assumes effectively a flat spectral index between 4.9 and 20 GHz. If instead we extrapolate with the median source spectral index $\langle \alpha \rangle \sim -0.4$ (0.1–2 mJy at 4.9 GHz) to the counts at 20 GHz, we find that the amplitude of the number counts is reduced from $K = 27.4$ to $K = 14.1$, and the expected rms to $\sigma = 49$ μK. Note that the true values of K and γ at high frequencies could differ from our extrapolations (by as much as 50% for K in particular) as is possibly indicated by more recent source counts at 8.4 GHz (Windhorst et al. 1992).

To investigate better the non-Gaussian aspects of the distribution, and verify the calculations of the rms ΔT using equation (21), we drew 50,000 Monte Carlo RING samples from a simulated 10° × 10° image (containing ~170,000 independent RING regions), using the above source counts, from which the distribution of RING σ_{tot} was determined. The rms value of σ_{tot} (see eq. [4c]) was found not to be robust over different images, due to the strong influence of the rare-event tail. The percentile points of the distribution, on the other hand, were found to be reliable. For all trials from the test image using the 4.9 GHz counts of $K = 27.4$ and $\gamma = 2.18$, we found a median $\sigma_{\text{tot}} = 132$ μK and a ninety-fifth percentile of $\sigma_{\text{tot}} = 859$ μK, demonstrating the extreme non-Gaussian behavior of source confusion. It must be realised, however, that most of the tail events that contribute to this large rms would have been seen in the RING as strong detections. To take account of this, we can "condition" the Monte Carlo trials to lie within the extremes of ± 439 μK of the RING data. The results of this should agree with the rms estimates above using the 1.74 mJy cutoff. We find 25.4% of the full 50,000 trial to be within the RING extremes, and a stable conditional median $\sigma_{\text{tot}} = 69$ μK, consistent with our earlier Poisson estimate, with a ninety-fifth percentile of 95 μK. This is a large fraction of the excess rms signal of 133 μK estimated from the maximum likelihood analysis. If the median spectral index is used to extrapolate the 4.9 GHz counts to 20 GHz ($K = 14.1$), then we find for all 50,000 trials a median $\sigma_{\text{tot}} = 75$ μK and a ninety-fifth percentile of $\sigma_{\text{tot}} = 514$ μK. For the 49.6% of the total trials with rms values between ± 439 μK we find a median of 50 μK, again consistent with our rms estimation, and a ninety-fifth percentile of $\sigma_{\text{tot}} = 77$ μK.

We can in principle invert the problem and determine the source counts from the RING rms excess. If we assume a slope of $\gamma = 2.18$ indicated by the 4.9 GHz counts, then we can solve equation (22) for K given a value of σ. For the MLM RING excess of $\sigma = 133$ μK (530 μJy), we find $K = 103$. If we use the Bayesian HPD 95% lower limit of $\sigma = 103$ μK (410 μJy), we find $K = 62$. These values are significantly higher than the range allowed by the 4.9 GHz VLA measurements. Furthermore, only 4.4% of the Monte Carlo trials using $K = 62$ fall within the RING measurement range. A Monte Carlo analysis similar to that detailed above was used by Wall et al. (1982) to investigate the results of a single-switching experiment. They were able to place reasonable limits on the amplitude K and slope γ of the counts using a χ^2 distribution comparison procedure because they had many more sample points. The linked nature and small size of the RING makes this much more difficult. A more detailed probabilistic treatment of the source counts for the RING will appear in a later paper.

In summary, it is likely that nonthermal extragalactic radio source contamination is responsible for a significant fraction, if not all, of the observed excess rms of 103–168 μK seen in the RING. A conservative estimate based upon the direct 5 GHz counts would give a 95% confidence contribution of 95 μK, heavily conditioned upon the RING maximum and minimum limits. The spectral-index extrapolated counts give a value of 77 μK, still a substantial fraction of the observed excess. Given the extreme non-Gaussian nature of the counts, and the uncertainty of the extrapolation to higher frequency, direct measurement of sources in the RING region is necessary to determine precisely the amount of contamination.

4.2. *VLA* 1.4/8.5 GHz *Survey*

Unfortunately, there is no existing deep radio survey which covers the entire region of the sky covered by the RING. For the NCP fields, we used a survey of the 5C9 field at 5 GHz (Pauliny-Toth et al. 1978) to identify contaminating sources. To fill in the unexamined regions, we have undertaken a survey of the north celestial polar cap region at 1.4 GHz, of the NCP main and reference fields at 5 GHz, and of the RING fields at 8.5 GHz, of the NCP main and reference fields at 5 GHz, and of the RING fields at 8.5 GHz. The observations were made at the VLA in the C-configuration. The data were taken and reduced using a procedure similar to that in previous VLA snapshot surveys (Condon, Condon, & Hazard 1982). We summarize here the 1.4 and 8.5 GHz observations that are directly relevant to the RING experiment; details will be published separately.

The 1.4 GHz images cover the area $\delta > 85°$ with 19″ FWHM resolution and a 32′ FWHM field of view. The largest distance of any interior point from a field center is 15′. After CLEANing, the images were searched for sources above the 6 σ noise level and within the 20% response of the primary beam. We identified 10 sources within 2.5 of a RING field center. In particular, we find two within 1′ in fields NPR1130 and NPR1700. The noise level in a VLA map at the position of an average RING field is ~700 μJy, while the error bar on an average RING field at 20 GHz is ≈480 μJy. Many sources are likely to have been missed at this frequency. Note that the

TABLE 6

VLA-RING 1.4/8.5 GHz SOURCE CATALOG

Source	$S_{8.5}$ (mJy)	$S_{1.4}$ (mJy)	$\alpha_{1.4}^{8.5}$	S_{20} (mJy)	f^{-1}	T_{est} (μK)
NPR0415.1	5.92 ± 0.11	22.6 ± 1.3	-0.75 ± 0.08	3.11 ± 0.41	12.2 ± 2.4	64 ± 16
NPR1130.1	3.59 ± 0.13	16.9 ± 1.4	-0.87 ± 0.08	1.70 ± 0.25	1.6 ± 0.1	267 ± 45
NPR1345.1	0.59 ± 0.08	1.4 ± 0.5	-0.48 ± 0.22	0.39 ± 0.12	2.5 ± 0.4	39 ± 14
NPR1700.1	4.50 ± 0.42	29.3 ± 2.3	-1.05 ± 0.09	1.82 ± 0.39	1.6 ± 0.1	286 ± 66

conversion factor between flux density and on-sky brightness temperature is given by the gain $g = 0.251$ K Jy^{-1} (see § 2).

In order to gain sensitivity and obtain measurements closer to our observing frequency, we observed 20 RING fields in two 6 minute scans each at 8.5 GHz with the VLA in the C-configuration. We observed those fields exhibiting the largest signals in the RING survey plus a few adjacent fields: NPR0015, NPR0030, NPR0045, NPR0415, NPR0700, NPR0830, NPR0845, NPR0900, NPR1015, NPR1130, NPR1145, NPR1345, NPR1700, NPR1930, NPR1945, NPR2000, NPR2045, NPR2115, NPR2130, and NPR2145. The average instrumental noise per field in the final images was 58 μJy (1 σ). The maps covered the 5'.3 FWHM field of view with a synthesized beam of 3" FWHM. In the final 8.5 GHz images, we found 18 sources within the 20% response level of the fields. All sources seen at 1.4 GHz in these fields were also detected at 8.5 GHz, and for the remaining 8.5 GHz sources the 1.4 GHz images were reexamined for sources at the 3 σ level and above. Spectral indices of $\alpha_{1.4}^{8.5}$ were determined for objects found at both frequencies. Unfortunately, the sensitivity limit of the 1.4 GHz survey is such that we detect mostly the steep spectrum sources of the 8.5 GHz sample and place only upper limits on $\alpha_{1.4}^{8.5}$ for flat spectrum objects. Sources at 1.4 GHz for which there were no corresponding 8.5 GHz images were removed from the sample pending completion of the RING 8.5 GHz survey; however, no significant fluctuations were seen in these fields at 20 GHz.

Using the spectral indices $\alpha_{1.4}^{8.5}$, flux densities were extrapolated to 20 GHz and converted to estimated RING temperature T_{est}. We find four of these 20 fields possibly contaminated with $T_{est} > 25$ μK: NPR0415, NPR1130, NPR1345, and NPR1700. The measured VLA flux densities and extrapolated 20 GHz intensities for these objects are given in Table 6. The beam attenuation factor f^{-1} calculated using the distance from the RING pointing center was used to determine the contribution to the RING measurements. The estimated signals from the objects in NPR1130 and NPR1700 are very close to the observed temperatures in the RING, while the sources in NPR0415 and NPR1345 have extrapolated strengths too low to account for the observed signals. In the case of NPR0415, the double structure seen in the 8.5 GHz images may indicate that assumption of a single α for both 8.5 GHz components is misleading. Because that source is 1'.6 from the field center and thus is 10 times stronger than measured at the RING pointing position we were able in 1989 December to make direct measurements at 20 GHz with the 40 m telescope. The temperature was found to be 1431 ± 92 μK corresponding to a flux density of 6.43 ± 0.52 mJy at 20 GHz. The spectral index $\alpha_{8.5}^{20}$ is 0.10 ± 0.15, significantly flatter than the $\alpha_{1.4}^{8.5}$ index. The temperature corrected to the RING position is 164 ± 49 μK, much closer to the observed RING value of 318 ± 114 μK. Although the direct measurement suggests that most, if not all, of the signal seen in NPR0415 is due to this source, it is an unfortunate fact that flat spectrum sources are nearly always variable sources, and reliable subtraction would require high-resolution 20 GHz observations simultaneous with the low-resolution microwave background measurements.

When calculating the contribution of point sources to the RING measurements we must also take into account the actual beam response pattern and the 14'.4 declination offset of the true reference field center from the adjacent RING field pointing center. We have used the beam map (see Fig. 2 in Paper 1) to obtain the factor f^{-1} needed to obtain the projected RING temperature equivalent T_{est}. The results for the four sources with $T_{est} > 25$ μK are shown in Table 7, for the fields where the object is in the main and reference beams. We find that the three sources NPR0415.1, NPR1130.1, and NPR1700.1 account for the signals seen in these fields, with reasonable residuals. For NPR0415.1, we have used the 20

TABLE 7

ESTIMATED CONTAMINATION OF RING FIELDS

Source	Field	f^{-1}	T_{est} (μK)	T_{RING} (μK)	T_{res} (μK)
NPR0415.1	NPR0400	-11.8 ± 2.7	-121 ± 30	-213 ± 113	-92 ± 117
	NPR0415	8.7 ± 2.5	164 ± 49	318 ± 114	153 ± 124
	NPR0430	-33 ± 12	-43 ± 16	-82 ± 112	-38 ± 113
NPR1130.1	NPR1115	-3.4 ± 0.3	-126 ± 23	-132 ± 113	-7 ± 115
	NPR1130	1.6 ± 0.1	267 ± 45	280 ± 114	14 ± 123
	NPR1145	-3.1 ± 0.2	-138 ± 23	-416 ± 101	-278 ± 103
NPR1345.1	NPR1330	-2.9 ± 0.3	-34 ± 11	-29 ± 102	5 ± 103
	NPR1345	2.5 ± 0.4	39 ± 14	271 ± 101	231 ± 102
	NPR1400	-4.0 ± 0.6	-24 ± 8	-202 ± 110	-178 ± 110
NPR1700.1	NPR1645	-2.8 ± 0.2	-163 ± 38	-220 ± 105	-57 ± 111
	NPR1700	1.6 ± 0.1	286 ± 66	342 ± 121	56 ± 138
	NPR1715	-3.4 ± 0.3	-134 ± 32	-233 ± 116	-98 ± 120

GHz measurement of the previous section, and after subtraction find that we have removed nearly all of the fluctuations in the three fields. Because of variability, it could be that the T_{est} derived above is an underestimate—a value 85% larger would leave only a residual of 11 μK rms among the three fields. A larger flux density for the source NPR1345.1 would also account for the observed RING signal in that field.

We are left with unexplained signal in NPR0700 and NPR1015 and an underlying variance below the detection level for single fields. It is possible that NPR0700 and NPR1015 contain sources with spectra rising from 8.5 to 20 GHz. Of these two fields, NPR0700 is the most convincing. It is flanked by negative fields and shows a 5.2 σ signal after matched filtering. This point will be discussed in the next subsection. Field NPR1015 is only a 3.0 σ "detection" after filtering, without the strong indication of negative "sidelobes" expected for a real source.

We conclude that the fluctuations in fields NPR0415, NPR1130, NPR1700, and possibly NPR1345 are due to the presence of identified discrete radio sources. Variability of the confusing objects would make correction of the RING unreliable, although examination of the residuals in Table 7 lends credibility to the estimates of the source strengths. If we use the corrected values (Table 7) for the above four fields, then we find the HPD limits for the rms signal

$$\begin{aligned} 79 < \sigma_{sky} < 144\ \mu K \quad (95\%) \\ 59 < \sigma_{sky} < 169\ \mu K \quad (99.87\%)\ . \end{aligned} \qquad \hat{\sigma}_{sky} = 110\ \mu K \qquad (23)$$

We have removed 48 μK rms from the RING data in these four fields, which reduced the MLM excess signal (8) from 133 to 110 μK. Correction of NPR0700 and the adjacent fields for the matched filter estimated signal of 466 ± 90 μK would remove another 59 μK, giving us the HPD limits

$$\begin{aligned} 60 < \sigma_{sky} < 127\ \mu K \quad (95\%) \\ 33 < \sigma_{sky} < 153\ \mu K \quad (99.87\%)\ . \end{aligned} \qquad \hat{\sigma}_{sky} = 93\ \mu K \qquad (24)$$

A complete survey of the 96 RING fields at 8.5 GHz with the VLA, along with 15 GHz and 20 GHz VLA observations of NPR0700 and NPR1015, has recently been completed. These results will be published in a separate paper. The new VLA data will provide better source counts for comparison and prediction purposes. At this time, we will consider the "corrected" RING used to obtain equation (23) to be our best data set, while noting the inclusion of the suspicious field NPR0700 and its contribution to the variance.

4.3. *Identification of NPR0700*

RING field NPR0700 contains the largest fluctuation in both the raw (Fig. 4 and Table 4) and matched-filtered data (Fig. 8). From the latter we estimate the "true" signal to be 466 ± 90 μK. Because it is both the brightest field in the survey and because it exhibits the characteristic "triple" signature expected for a real source, NPR0700 merits special attention. Although one 3 σ or greater deviation would be expected at the 12% level in a sample of this size, the 5.2 σ amplitude of the filtered signal in NPR0700 makes it unlikely that it is due to noise. The lack of an overall bias in the RING mean level argues against a systematic error in the measurement as the explanation. We now explore the astronomical possibilities for the nature of this object.

Because four of the seven candidate fields were found to contain nonthermal discrete radio sources, we first consider the available limits on such an object in the field of NPR0700. The equivalent flux for NPR0700 (from the filtered data) is 2.1 ± 0.4 mJy at the beam center. We find in the 8.5 GHz VLA images only a single 0.45 mJy source, located 1.'4 from the field center (effective flux density 88 μJy). The 1.4–8.5 GHz spectral index is found to be $\alpha = -0.9 \pm 0.4$, although the 8.5–20 GHz spectrum may flatten like that of NPR0415.1. Thus, if this object is responsible for the signal we have detected in NPR0700, then a strongly inverted spectrum ($\alpha = 3.7$) would be required from 8.5–20 GHz, which is unlikely for extragalactic sources. It is possible that NPR0700.1 is highly variable, or that an undetected source in the center of the field is responsible. The central noise level of the 8.5 GHz VLA image is 360 μJy (6 σ), thus requiring a spectral index of $\alpha > 2.0$ for such a source. This is an extreme value, but because we are selecting this "object" based on its 20 GHz flux density, it should not be ruled out entirely. In the 4.9 GHz data (Fomalont et al. 1991) there were 10 out of 68 sources with $\alpha_{1.4}^{4.9} > 0.3$, of which one had $\alpha_{1.4}^{4.9} > 1.2$. For sources selected at 8.5 GHz, approximately 30% of sources in this flux range are found to have flat or inverted ($\alpha \sim 1.0$) spectra (Fomalont et al. 1992), Further VLA observations at 20 GHz should settle this question easily.

Another possibility is that a bright radio source in a far sidelobe of the OVRO beam is causing the signal in NPR0700, and could be a contributor to the other excess variance in the RING data. It is unfortunately impossible to measure the low-level sidelobes of the combined receiver and telescope response pattern reliably. We are currently investigating the dependence of the NPR0700 and NPR1015 signals on the orientation of the beam switching direction on the sky, using new observations that track these fields over the full hour-angle range, which should reveal the presence of a confusing source outside the main beam.

Galactic dust emission is another candidate for a contaminating foreground source. Dust emission can be characterized by a modified blackbody spectrum $I_\nu \sim \nu^p B_\nu$, where $B_\nu(T_d)$ is the intensity for a blackbody at temperature T_d and p the emissivity index. The *COBE* measurements of dust in the Galactic plane estimate a dust temperature of $T_d = 23.3$ K and emissivity index of $p \sim 1.65$ for a single-component fit (Wright et al. 1991). The signal in NPR0700 corresponds to an intensity of $\Delta I_\nu = 4750$ Jy sr^{-1} at 20 GHz, which implies $\Delta I_\nu = 5460$ MJy sr^{-1} in the *IRAS* band at 100 μm. If the dust were significantly colder, say $T_d = 10$ K, then the implied intensity would drop to $\Delta I_\nu = 3.5$ MJy sr^{-1} at 100 μm. If the emissivity index were to increase to $p = 2$, then the required intensities would be increased by a factor of 5.8, while $p = 1$ would decrease these values by a factor of 26. Typical intensities for the diffuse galactic emission as measured by *IRAS* are 13 MJy sr^{-1} (at 100 μm) in the South Galactic pole region (Hauser et al. 1984). Also, 100 μm emission from infrared cirrus with structures on scales of $\sim 0.^\circ 3$–$2.^\circ 5$ is seen with $\Delta I_\nu = 1$–10 MJy sr^{-1} and $T_d \sim 26$–34 K (Low et al. 1984). It is thus unlikely that the observed signal in NPR0700 is due to the IR cirrus, unless dust temperatures of ~ 10 K are common. Higher frequency observations at 90 GHz are planned to discriminate against dust emission as a foreground source.

Galactic synchrotron emission, which may be responsible for contamination of the Tenerife experiment (Banday & Wolfendale 1989; Banday et al. 1991) is characterized by a spectral index of $-0.7 < \alpha < -0.5$ in the north polar region (Lawson et al. 1987), and for a source at the beam center would imply a

flux density of 2.7–4.5 mJy at 8.5 GHz and 4.7–23 mJy at 1.4 GHz. However, galactic emission is likely to be extended, and the VLA snapshot observations have poor sensitivity to such sources. In the 8.5 GHz images, the sensitivity ranges from 360 μJy (6 σ) at 3″ resolution to 1.0 mJy (6 σ) at 15″. Beyond around 1′, the structure is effectively resolved out by the array due to the very limited spatial-frequency coverage in the snapshot. Because it exhibits strong negative sidelobes in the RING data, the source cannot be much larger in radius than the switching angle 7.′15. The 1.4 GHz noise level at the position of NPR0700 is 6.5 mJy (6 σ) for a resolution of 19″. The data are sensitive to sources with angular sizes less than 7′. It is thus possible for an extended synchrotron source to cause the 20 GHz signal while escaping detection in the VLA images, especially for angular sizes $\theta_D > 2'$.

A fourth possibility, the most interesting in the context of cosmology, is that NPR0700 contains a fluctuation in the microwave background radiation. This would have a thermal spectrum with the CMBR temperature at all wavelengths. The VLA 8.5 GHz images place poor limits on the strength and scale of these fluctuations, since the microwave background flux density is $1.5\theta''^2_{\rm fwhm}$ μJy. Using the 6 σ limit in the NPR0700 field of 1 mJy at $\theta_{\rm fwhm} = 15''$, we find a limit of $\Delta T/T < 3 \times 10^{-2}$ (6 σ) on this scale. Because the flux density from a thermal source scales with ν^2 in the Rayleigh-Jeans limit, higher frequency observations will have a better chance of confirming a background fluctuation.

Each of these possibilities is interesting astronomically, yet one must be cautious at drawing strong conclusions from the incomplete data at hand. Follow-up observations at 20 GHz with OVRO are underway, as are further 15 and 8.5 GHz observations with the VLA. All of these explanations must be seriously considered, and the VLA as well as millimeter and submillimeter wavelength observations will serve to distinguish between them. At this point we will conclude that there is a strong possibility that field NPR0700 contains an unusual radio source, either background or foreground in origin. Pending identification of this object, we will leave this field uncorrected in the subsequent analysis.

5. DISCUSSION

We have shown that the RING data set has greater variance than expected from the contributions of the instrumental and atmospheric noise alone. The MLM rms amplitude of this signal is $\hat{\sigma}_{\rm sky} \sim 133$ μK. Through matched filtering, seven fields (NPR0415, NPR0700, NPR1015, NPR1130, NPR1345, NPR1700, NPR1945) with fluctuations above 3 σ were identified, and of these, four (NPR0415, NPR0700, NPR1130, NPR1700) showed significant deviations from zero in the positive MEM reconstruction. Based on VLA observations, at least three RING fields (NPR0415, NPR1130, NPR1700) are strongly contaminated by discrete radio sources. After the VLA source subtraction, several fields remain with deflections above the 10^{-4} level, most notably NPR0700 and NPR1015, but the MLM amplitude of the excess signal drops to $\hat{\sigma}_{\rm sky} =$ 110 μK. The corrected field values for the RING are shown in Figure 10, in units of the microwave background temperature $T_{\rm mwb} = 2.735$ K (Mather et al. 1990; Gush, Halpern, & Wishnow 1990).

5.1. *Generalized Gaussian Fluctuation Models*

We first deal with generalized forms for Gaussian random fluctuations. Because the RING is interlocked, we have the

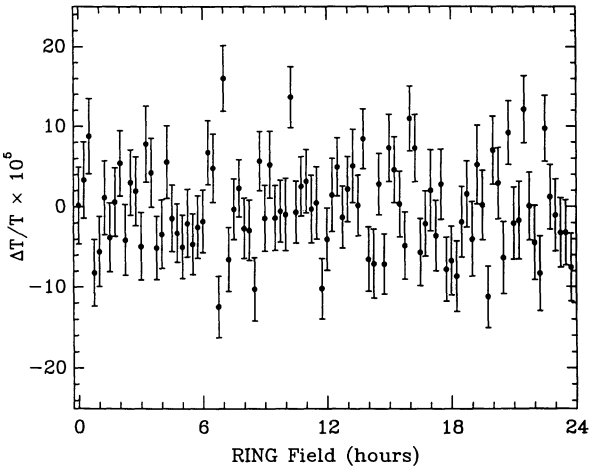

FIG. 10.—Corrected RING measurements with estimated contributions from the VLA 8.5 GHz radio sources subtracted, expressed as a fraction of the microwave background temperature $T = 2.735$ K.

vector relation between the data $\boldsymbol{y}$, the intrinsic sky samples $\boldsymbol{x}$, the switching matrix A, and the measurement errors $\boldsymbol{e}$ given by

$$\boldsymbol{y} = A\boldsymbol{x} + \boldsymbol{e} \tag{25}$$

where $x_j = T_j$ is the true temperature of the sky in beam j, and $y_i = \Delta T_i$ is the measured temperature difference for the RING field with pointing center at x_i, e_i is the error, and A is the sampling matrix

$$A_{ij} = \delta_{ij} - \tfrac{1}{2}\delta_{ij-1} - \tfrac{1}{2}\delta_{ij+1} \,. \tag{26}$$

The field indices u and j are taken modulo 96. Note that A is singular and in fact has one zero eigenvalue corresponding to the unmeasured mean value.

We assume that points $\boldsymbol{x}$ sample a real-valued Gaussian random field F defined over the two-dimensional sky $x_i = F(\boldsymbol{r}_i)$. The distribution function for the multivariate $\boldsymbol{x}$ is (Kendall & Stuart 1977)

$$P(\boldsymbol{x}) = (2\pi)^{-n/2}(\det C)^{1/2} \exp\left[-\tfrac{1}{2}(\boldsymbol{x} - \boldsymbol{u})^T C^{-1}(\boldsymbol{x} - \boldsymbol{u})\right] , \tag{27}$$

where the correlation matrix C is given by

$$C_{ij} = \langle (x_i - \mu_i)(x_j - \mu_j) \rangle \,, \tag{28}$$

and vector $\boldsymbol{u} = (\mu_1, \ldots, \mu_n)$ is the mean vector. For the RING, $n = 96$. Because $\boldsymbol{x}$ is sampled from the Gaussian random field F, assumed to be homogeneous and isotropic, the $\mu_i = \mu$ are identical, and the elements of C are functions only of the relative angle ϕ_{ij} between the locations of the sample points: $C_{ij} = C(\phi_{ij})$. Because our switching matrix A_{ij} is singular and we are insensitive to a mean level, we can take $\mu = 0$ without loss of generality.

Our microwave background temperature field $F(\boldsymbol{r})$ is defined on the celestial sphere, with the angular coordinates $\boldsymbol{r} = (\alpha, \delta)$. While it is convenient for consideration of angular scales larger than a few degrees to use Legendre polynomials C_ℓ, for small angles $\phi \ll \pi$, with modes $\ell \gg 1$ dominating, we can use the standard Fourier transform

$$C(\phi) = \frac{1}{4\pi} \sum_\ell (2\ell + 1) C_\ell P_\ell(\cos\phi) \,, \tag{29a}$$

$$\simeq \frac{1}{2\pi} \int_0^\infty \ell \, d\ell \, C_\ell J_0(\ell\phi) \,. \tag{29b}$$

From this, we can construct the correlation function $C(\phi)$ and correlation matrix C_{ij} from the power spectrum C_ℓ.

To obtain the probability distribution for our data points, and hence the likelihood function, we need to include the observational filtering. We follow the methodology of Paper 1 (§ VIIIb) and consider the random field F_s as the true field F "smeared" by the finite telescope resolution: $x_i = F_s(r_i)$. We approximate our antenna response pattern by a circularly symmetric Gaussian with dispersion $\phi_0 = 0.^\circ764$. The limitations of this approximation were discussed previously in § 2 and in Paper 1 (§§ II, VIIIc), and it is clear that the deviations from symmetry and Gaussian profile are not significant for distributed fluctuations on angular scales of importance here. The correlation function of F_s is the convolution of the correlation function of the beam and that of F; for our Gaussian beam we denote this $C(\phi_0, \phi)$. The transforms are related by

$$C_\ell(\phi_0) = C_\ell e^{-\phi_0{}^2\ell^2} . \tag{30}$$

The two-point correlation matrix U for $\boldsymbol{y}$ is related to the matrix C for $\boldsymbol{x}$ by

$$U = A^T C A + E \tag{31}$$

with the diagonal error matrix $E_{ij} = \epsilon_i^2 \delta_{ij}$. We assume that the errors e_i for each field y_i are drawn from a $N(0, \epsilon_i^2)$ normal distribution.

The simplest model for the anisotropic component of the microwave background as measured by the NCP and RING experiments is a Gaussian random field without spatial correlation between patches of sky and the size of the OVRO 20 GHz primary beam (108″ FWHM), between which there is a variance c_0. In this case, we can write $C_{ij} = c_0 \delta_{ij}$. For the RING, the switching matrix A is banded and symmetric, so that

$$U_{ij} = [\tfrac{3}{2}C_{ij} - (C_{ij-1} + C_{ij+1}) + \tfrac{1}{4}(C_{ij-2} + C_{ij+2})] + \epsilon_i^2 \delta_{ij} . \tag{32}$$

Note that the RING field indices wrap around at $i = 0$ and 96, and there are nonzero entries in the corners of the matrix. We can then perform our calculation of the HPD limits using for the likelihood

$$L(\theta) = (2\pi)^{-n/2} (\det U)^{-1/2} \exp(-\tfrac{1}{2}\boldsymbol{y}^T U^{-1} \boldsymbol{y}) . \tag{33}$$

We take as our integration variable the amplitude of the rms fluctuation $\theta = c_0^{1/2}$. For the uncorrected RING data, we obtain the 95% and 99.87% (3 σ) HPD limits of

$$\begin{aligned} 3.0 < \frac{\Delta T}{T} < 5.4 \times 10^{-5} \quad (95\%) \\ 2.4 < \frac{\Delta T}{T} < 6.5 \times 10^{-5} \quad (99.87\%) . \end{aligned} \qquad \frac{\Delta \hat{T}}{T} = 4.1 \times 10^{-5} \tag{34}$$

If we use the corrected RING data set with the estimated contributions from the known VLA sources removed, then the HPD limits are

$$\begin{aligned} 2.3 < \frac{\Delta T}{T} < 4.5 \times 10^{-5} \quad (95\%) \\ 1.6 < \frac{\Delta T}{T} < 5.5 \times 10^{-5} \quad (99.87\%) . \end{aligned} \qquad \frac{\Delta \hat{T}}{T} = 3.3 \times 10^{-5} \tag{35}$$

These limits (34) and (35) differ from those given in equations (23) and (24) respectively by a factor of $\sqrt{1.5}$, due to the factor in the definition of the correlation matrix equation (32). The limits from the RING corrected data can be compared with the Bayesian upper limits from the NCP experiment; as in § 3.1 we find disagreement between the NCP 95% upper limit (1.7×10^{-5}) and the RING 95% lower limit (2.3×10^{-5}), but marginal agreement between the 99.87% upper limit (3.8×10^{-5}) for the NCP and 99.87% lower limit (1.6×10^{-5}) for the corrected RING. This suggests, although not strongly, that uncorrelated Gaussian fluctuations are *not* the cause of the excess variance in the RING data.

If we are to use the spatial information provided by the switching matrix, we need to assume some form for the autocorrelation function $C(\phi)$ of the fluctuation model. A common, and tractable, assumption is that $C(\phi)$ can be approximated as a Gaussian over the angular scales of importance

$$C(\phi) = c_0 \exp\left(-\frac{\phi^2}{2\phi_c^2}\right) \Leftrightarrow C_\ell = 2\pi\phi_c^2 c_0 e^{-(1/2)\theta_c{}^2\ell^2} , \tag{36}$$

where

$$\phi_c = \left[-\frac{C(0)}{C''(0)}\right] . \tag{37}$$

We can then calculate the limits on the amplitude $c_0^{1/2}$ as a function of the coherence angle ϕ_c. It should be noted that this approximation is not very accurate for most realistic models, but provides a simple illustration of the sensitivity of the experiment for models with different characteristic fluctuation scales.

The angular distances ϕ_{ij} between the field centers of x_i and x_j in the RING are given by

$$\cos\phi_{ij} = 1 - \left[1 - \cos\left(\frac{\pi\Delta_{ij}}{48}\right)\right] \cos^2\delta \tag{38}$$

for RING declination $\delta = 88^\circ10'42''$ with

$$\Delta_{ij} = \begin{cases} |i-j| & 0 \le |i-j| \le 48 \\ 96 - |i-j| & 48 < |i-j| \le 96 . \end{cases} \tag{39}$$

The correlation matrix C must then be constructed using the smeared autocorrelation function $C(\phi_0, \phi)$ from equations (36) and (30)

$$\begin{aligned} C(\phi_0, \phi) &= \frac{c_0 \phi_c^2}{2\phi_0^2 + \phi_c^2} \exp\left[-\frac{\phi^2}{2(2\phi_0^2 + \phi_c^2)}\right] \Leftrightarrow C_\ell(\phi_0) \\ &= 2\pi\phi_c^2 c_0 e^{-1/2(2\phi_0{}^2 + \phi_c{}^2)\ell^2} . \end{aligned} \tag{40}$$

Because the reference beams in a given RING switched field measurement are very nearly centered on the adjacent field's main beam, we can construct $C_{ij} = C(\phi_0, \phi_{ij})$ and insert in equation (32). Note that C is an implicit function of the free parameters $c_0^{1/2}$ and ϕ_c.

The likelihood function (35) can be evaluated numerically for a lattice of $(c_0^{1/2}, \phi_c)$. Because there are significant correlations between the fields, especially for large values of ϕ_c, the matrices C and U are no longer sparse. The $(1 - \alpha)$ HPD limits were determined by finding the smallest interval in $c_0^{1/2}$ containing the highest values of L for which the integral is greater than or equal to a fraction $(1 - \alpha)$ of the total integrated L. The results for $(1 - \alpha) = 0.95$ and $(1 - \alpha) = 0.9987$ are shown for the uncorrected RING data in Figure 11*a*. The solid curves represent the HPD upper and lower limits on the amplitude

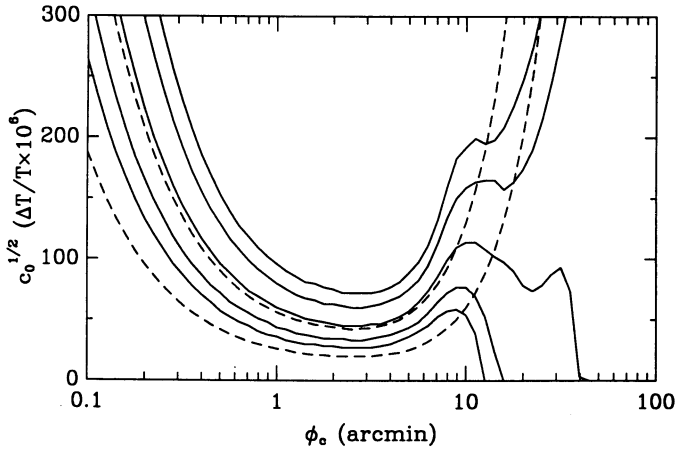

FIG. 11*a*

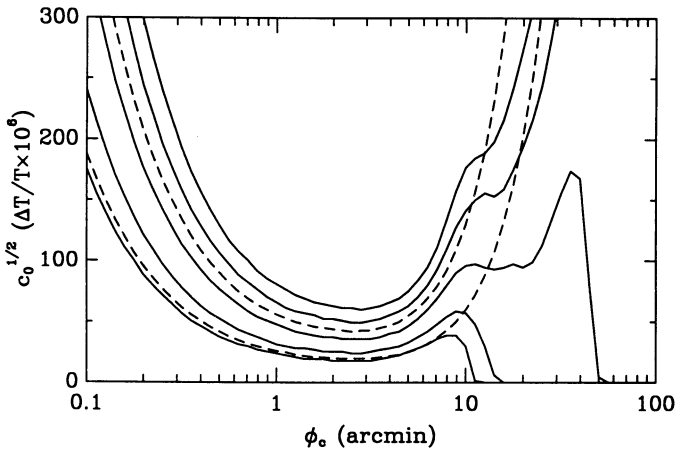

FIG. 11*b*

FIG. 11.—Bayesian 95% and 99.87% HPD upper and lower limits on and MLM estimate of the rms fluctuation amplitude $c_0^{1/2}$ in the (*a*) original RING data and (*b*) the corrected RING data, for the Gaussian autocorrelation function model with coherence angle ϕ_c. The center solid curve is the MLM estimated value and is flanked by the 95% limits, with the two outside solid curves showing the 99.87% limits. Also shown are 95% (*lower dashed*) and 99.87% (*upper dashed*) HPD upper limits from the NCP experiment.

$c_0^{1/2}$ and the MLM value $\hat{c}_0^{1/2}$. Also superposed on the limits are the 95% and 99.87% upper limits from the NCP experiment (dashed curves). The finite resolution of the numerical grid ($\Delta = 1.5 \times 10^{-6}$) can be seen in the figure, as well as some possible artifacts, especially where the limit changes from two-sided to one-sided. The level of disagreement between the NCP upper limits and the RING lower limits can also be seen. From the figure, we see that at the 95% level, the NCP upper limit is consistent with the RING lower limit for coherence angles $\phi_c > 10'$, while the 99.87% limits are more or less consistent over the entire range of angles.

In Figure 11*b*, the same curves are shown for the corrected RING data. The NCP 95% upper limit is consistent with the RING 95% lower limit for $\phi_c > 7'$, and relatively close over most of the range of angles. For coherence angles above 20′ the linked RING geometry provides better 95% upper limits than the sparse NCP sampling, despite the lower sensitivity per field. For the 99.87% limits, the RING provides the beter limit for angles $\phi_c \geq 13'$.

5.2. *Comparison with Specific Gaussian Models*

In the discussion of the predictions of a selection of published galaxy formation models for the NCP experiment given in Paper 1 (§ X and Table 6), 56% of the models considered were ruled out at the 95% confidence level, and a further 20% were within a factor of 2 of exclusion by the NCP results. By and large, the most successful models were those involving $\Omega = 1$ and a dominant cold dark matter (CDM) component, or significant early reionization of the universe after recombination. For adiabatic CDM models, the OVRO NCP limits restrict the allowed range for the linear biasing parameter $b_8 = 1/\sigma_8$, where σ_8 is the rms mass overdensity within a sphere of radius 8 h^{-1} Mpc. This is also related to the alternate biasing parameter b_ρ used in some of the references (e.g., Bond 1988a), where $b_8 \approx 1.073 b_\rho$. The isocurvature models with early reionization are also not excluded by our previous 95% limits (see the review in Bond 1988b) as even rather low ionized fractions (<10%; see Table 6 in Paper 1 and Bond & Efstathiou 1987; Efstathiou 1988) affect anisotropies on arcminute scales. A prolonged recombination or subsequent early reionization will enlarge the width of the last scattering "surface" and thus increase the coherence angle of the fluctuation correlation function. If the universe never recombines, the angular scale increases from $\phi_c \sim 10'$ for standard recombination to $\phi_c \sim 5°$ (Bond 1988a). In the summary of adiabatic and isocurvature CDM and neutrino models without reionization by Holtzman (1989) only the $\Omega = 1$ models with small baryon fractions are not excluded by our results. Recent hybrid models with both hot and cold dark matter are very close to the NCP limit although a correct calculation has not been performed (Schaefer, Shafi, & Stecker 1989).

The recent experiment at the South Pole on angular scales 30′–1° (Meinhold & Lubin 1991), when combined with the OVRO NCP results, places severe limits on the biasing parameter b_8 for CDM models (Bond et al. 1991b; Vittorio et al. 1991; Bond & Myers 1992). For $\Omega = 1$ CDM models with $H_0 = 50$, $\Omega_B = 0.03$ and standard recombination, Bond et al. 1991 find that $b_8 > 0.48$ for the South Pole data alone, $b_8 > 0.46$ for the OVRO NCP, and $b_\rho > 0.71$ with the two combined at the 95% credible level. For $\Omega_B = 0.1$, the combined limit becomes $b_8 > 1.02$. Clustering and velocity correlations in large-scale structure constrain $0.85 < b_8 < 1.82$, and improvements in the limits on the angular scales spanned by these experiments will begin to constrain the parameter space available to these models. However, models with no recombination and $\Omega_B = 0.1$ are hardly constrained at all by these observatons, with $b_\rho > 0.29$ for the South Pole. The OVRO NCP places no constraints on these models, since the angular scale of the last scattering "surface" is around 5°, well above the range of this experiment. Large-angle measurements from balloon or *COBE*, as well as the new South Pole data, will test these models much more effectively (see § 7). Bond et al. 1991 also place limits on Ω_B and b_ρ for isocurvature models.

The results of the RING can also be added to the NCP and South Pole data to place further limits on these models, although the presence of the unidentified signal in the RING causes the resulting limits on b_ρ to loosen significantly (Bond & Myers 1992). The contradiction between the NCP 95% upper limits and the RING 95% lower limits would suggest that for Gaussian fluctuations (with a roughly Gaussian autocorrelation function), the coherence angle $\phi_c > 10'$. This is not a

strong limit, as the 99.87% limits from the two experiments are consistent. The upper limits from the Meinhold & Lubin (1991) experiment cast further doubt on the viability of such a model—certainly models with power spectra peaking near the South Pole angular scales, like CDM, would be unable to satisfy both the RING and South Pole limits at a reasonable confidence level.

It should be stressed once again that the nonzero lower limit indicated by the RING analysis should *not* be taken as conclusive evidence for the detection of microwave background anisotropy. Some significant contaminating signals due to nonthermal discrete radio sources have already been subtracted from the measurements, but it is certain that there is a nonnegligible level of contaminating signal remaining in the data set from objects missed in the 8.5 GHz VLA survey due to incomplete spatial coverage, inadequate sensitivity, inaccurate extrapolation of spectral energy distributions to 20 GHz, and insufficient knowledge of the OVRO primary beam at low levels which is needed for proper source modeling. In the light of these problems, it is advisable to use only the upper limits from the HPD analysis of the RING when investigating the predictions of cosmological models, unless and until the 3 σ candidate deviations in NPR0700 and NPR1015 are shown to be real, extended, and attributable to the microwave background. Despite the traditional use of the 95% "confidence" measure adopted in the literature and practice of the microwave background observational field, it is also prudent to use the more conservative 99.87% limits equivalent to a 3 σ deviation from a normal distribution. There is no advantage to using a 95% confidence limit, and it is more sensible to use the 3 σ limits as is standard in other areas of study.

5.3. *Comparison with Non-Gaussian Models*

Although the limits placed on Gaussian models are significantly poorer than those from the NCP experiment, the RING experiment provides increased sensitivity to certain classes of non-Gaussian models, as demonstrated by the greater vulnerability to contamination by discrete radio sources. For example, Poisson pointlike objects with a power-law differential number count index between 1 and 3 will have an increasing contribution to the variance as the number of fields observed is enlarged. There are a number of theories for the formation of galaxies and large-scale structure that predict some form of non-Gaussian behavior. We can divide these models roughly into two classes: those in which the primary fluctuations themselves are non-Gaussian at the time of their generation (e.g., during the epoch of inflation), and those in which the primary anisotropies are modified or exceeded by secondary fluctuations created by the effects of massive particles or structures in the early universe or after recombination. We will now briefly discuss the various scenarios in each class and estimates of the contribution to the anisotropy in the RING experiment where available.

The inflationary paradigm (Guth 1981; Linde 1982; Albrecht & Steinhardt 1982) has been successful at explaining the flatness of the universe and why the microwave background is isotropic to at least one part in 10^{-3} (other than the dipole term due to our peculiar velocity in the cosmic background frame), but it is by no means free of loose ends or fine-tuning problems. The generation of fluctuations with Gaussian statistics is taken to be a consequence of the required weak coupling of the "inflation" scalar field (see Wise 1988), but problems with the reconciliation of the standard model with the observed properties of large-scale structure have kindled interest in non-Gaussian primordial fluctuations (e.g., Peebles 1983). Single-field inflation produces Gaussian fluctuations on scales contained within the observable universe, but may break scale-invariance of the spectrum (Salopek, Bond, & Bardeen 1989). Inflation with more than a single scalar field may lead to non-Gaussian perturbation statistics in addition to breaking scale invariance (Kofman & Pogosyan 1988; Salopek, Bond, & Bardeen 1989), which allows an increased amplitude of long-wavelength fluctuations to produce large-scale structure and peculiar velocities. However, since no reliable theories exist that predict a scalar field whose potential surface has the required behavior for inflation, Gaussian statistics or not, there are no available quantifiable models for non-Gaussian fluctuations generated in these scenarios. A "toy model" using double-field inflation where non-Gaussian behavior enters through focusing of trajectories down the potential surface has been proposed by Salopek (1991), although no calculation of the statistical effect has been attempted.

A great deal of effort has been put into the investigation of nonbaryonic ingredients in the particle mix of the early universe, mostly with an eye toward assisting matter in the collapse into structure without causing excessive anisotropy in the microwave background. In the prevalent models with baryons plus a dominant nonbaryonic dark matter component the resulting fluctuations in the background remain Gaussian because the density perturbations are still in the linear regime at decoupling. Topological defects in the vacuum originating from the phase transition in the scalar inflation field at the end of inflation are inherently nonlinear, and the perturbations introduced in the baryonic component at and after recombination are therefore non-Gaussian. The one-, two-, and three-dimensional defects (boundaries between regions of space with different realized values of order parameters in a broken symmetry) are known as strings, domain walls, and texture. The density of domain walls separating regions of space containing different degenerate vacua resulting from a GUT transition is diminished by GUT-scale inflation, although there have been recent attempts to enlist walls in the formation of structure (Press, Ryden, & Spergel 1989). Texture is a newcomer to the exotic cosmological zoo and consists of regions of space in which the order parameter of a global symmetry has a fixed value (Turok 1989). By far, the most popular defects are cosmic strings, one-dimensional regions of false vacuum that possess a mass per unit length μ (see Vilenkin 1986 and references therein), and closed loops of strings are postulated to form seeds for the formation of galaxies. In addition to the induced density perturbations, cosmic strings act as gravitational lenses to modify directly the microwave background radiation, forming step discontinuities in the background temperature. Numerical simulations of anisotropies induced by string networks have been performed by Bouchet, Bennett, & Stebbins (1988) who have constructed maps of the resulting background temperature field. The limits derived for the NCP experiment using the rms string fluctuations are (from a Gaussian analysis)

$$\frac{G\mu}{c^2} \leq 2 \times 10^{-6} ; \tag{41}$$

however, as noted by the authors, non-Gaussian effects are likely to render this limit unreliable. Because galaxy formation

scenarios using strings as seeds require $G\mu/c^2 \sim 1\text{–}4 \times 10^{-6}$, the correct analysis of the RING and NCP limits for these models should provide important constraints on these models. Collapsed objects at moderate to high redshift may also alter the microwave background correlation spectrum through gravitational lensing effects (Cole & Efstathiou 1989), although this mechanism is unlikely to be effective on angular scales of interest to us.

The presence of dust or ionized gas in the universe after recombination will also modify the fluctuations in the microwave background temperature. The reports of an excess in the submillimeter region of the background spectrum of the 2.74 K blackbody, the latest being the Matsumoto et al. (1988) rocket experiment, spurred theoretical interest in models with significant amounts of dust at redshifts $x > 10$ (Bond, Carr, & Hogan 1986, 1991a; Djorgovsky & Weir 1990) wherein heating of dust by protogalactic objects or active galactic nuclei in the (moderately) early universe causes reradiation in the infrared bands which is then redshifted into the submillimeter wavelength range. The effect of these dusty objects on the anisotropy of the microwave background radiation depends on the Poisson statistics of the number counts of the sources. The OVRO NCP results, among others, place stringent limits on the density ($>30\ h^3$ Mpc^{-3}) or clustering ($<60\ h^{-1}$ kpc) of these sources (Hogan & Bond 1988; Bond et al. 1991a). However, the immediacy of these results has disappeared along with the submillimeter excess with the measurement of background spectrum by the *COBE* satellite FIRAS experiment (Mather et al. 1990) and the COBRA rocket experiment (Gush et al. 1990), which place a limit of 1% of the peak intensity on the deviation from a 2.735 K blackbody over the frequency range 30–600 GHz. Explosive galaxy formation scenarios (e.g., Ikeuchi 1981; Ostriker & Cowie 1981), like those involving superconducting cosmic strings (Ostriker, Thompson, & Witten 1987; Ostriker & Thompson 1987), also generate non-Gaussian secondary anisotropies, although it has been claimed that there is negligible heating of the pregalactic medium for efficient blast waves. There are no quantitative fluctuation distributions predicted by these models, although it is likely that they would resemble Poisson-seeded scenarios. In any event, comparison with the RING will require specific models.

Another set of secondary anisotropy-generating models are the decaying particle theories (e.g., Daly 1988; Doroshkevich, Klypin, & Khlopov 1989) where galaxy formation is prompted either through explosive decay of massive nonbaryonic particles or through gravitational clustering around these seeds, which later decay and disappear. The work on a condensate scenario by Daly predicts the number of detections for the RING experiment above the $\Delta T/T = 1 \times 10^{-4}$ level; four are found in the corrected data set. This places an upper limit on the volume filling factor of voids at the current epoch determined by her models of 0.02–0.09, while observations estimate the true value to lie in the range 0.03–0.13. Thus, these models are consistent with the data assuming the identified fields are not due to noise or to discrete radio sources.

Any process that releases significant amounts of energy at an early epoch after recombination will produce secondary anisotropies in the microwave background radiation as well as distort the blackbody spectrum. The limit from *COBE* on the total Compton y-parameter is $y < 0.001$ (Mather et al. 1990). In the Rayleigh-Jeans region of the microwave background spectrum the scattering of background photons off the electrons in the hot gas causes a decrement in the observed equivalent temperature at frequencies below the blackbody peak as the photons are preferentially scattered up in energy to the Wien region of the spectrum (cf. Sunyaev & Zel'dovich 1981). This process, known as the Sunyaev-Zel'dovich effect, has been observed at a level of 600 μK–1 mK in nearby clusters of galaxies with hot X-ray–emitting coronae (Birkinshaw, Gull, & Hardebeck 1984; Birkinshaw 1987) with the OVRO 20 GHz system. Various estimates of the cumulative effect upon the microwave background radiation by modeling of the formation and evolution of these clusters have been made. Schaeffer & Silk (1988) estimate the contribution to the Uson & Wilkinson (1984c) experiment to be $\sim 3 \times 10^{-5}$. Because the estimated correlation angle of the fluctuations was 1′, the contribution to the OVRO experiments should be slightly less than this, possibly near the level of the NCP limit. Cole & Kaiser (1989), in their CDM model, estimate the rms amplitude expected for the NCP experiment to be

$$\frac{\delta T}{T} \sim 5 \times 10^{-6} . \tag{42}$$

Other models are considered by Bond (1988a), who calculated distributions based on a model of cluster formation and evolution. The effect from ionized gas in explosions is also evaluated, producing fluctuation amplitudes of 10^{-6} to 4×10^{-5} on the scale of 10′. He points out that HDM models with "pancaking" at redshifts $z > 3$ are ruled out through limits on the Sunyaev-Zel'dovich effect.

Because the distribution of clusters is Poissonian in the absence of clustering, and the distortions to the microwave background are decrements only, the statistics of the fluctuations induced are non-Gaussian with a strong negative tail, and predictions for large sample experiments such as the RING are not easily estimated from simple calculations. Numerical simulations of galaxy formation in the popular CDM scenario are now beginning to include the evolution of the baryonic component as well as the dark matter and energy injection by protogalaxies into the gaseous medium, which can lead to non-Gaussian perturbations of the background radiation. Recent work by Ryu, Vishniac, & Chiang (1990) predicts fluctuations at the level $\sim 4 \times 10^{-6}$ with a log-normal distribution, although no specific experimental predictions are available. Bond & Myers (1992) have produced simulated images of the Sunyaev-Zel'dovich effect for CDM scenarios using a "hierarchical peaks" method for determining the distribution and evolution of virialized clusters and groups. Monte Carlo simulations of the OVRO surveys based on this method predict that the probability of finding one or more fields with a fluctuation above 3 σ in either the NCP or RING is less than 1% for even the $b_\rho = 1$ models. It is unlikely that the secondary anisotropies due to the hot gas in these models is a significant contributor to either the RING or the NCP, outside of the rare bright clusters.

We have outlined a number of theoretical models that predict non-Gaussian fluctuation distributions of possible interest to us for comparison with the RING and NCP experiments. With the exception of Daly's condensate and decay model, and the Sunyaev-Zel'dovich models, none of the scenarios discussed have presented sufficient information on the distributions to permit detailed statistical analyses similar to those for Gaussian models. In Bond & Myers (1992), Monte Carlo sampling of a single simulated sky map yielded a reasonable comparison with the OVRO measurements. However, the

size of the image was too small to simulate the entire RING geometry, and the quoted probabilities were calculated by taking 96 randomly located points. It is not yet apparent whether even Monte Carlo tests using the full RING can effectively deal with the cross-correlations between the fields without an excessive number of trials and a large map area. Work continues on this problem, and on the general question of analysis of non-Gaussian model distributions.

There are some possibilities for testing sparsely sampled data such as the RING observations for the signature of non-Gaussian statistics, although the presence of instrumental noise complicates the problem considerably. The Kolmogorov-Smirnov test of the RING field distribution revealed that the data were marginally inconsistent with a Gaussian distribution assuming no sky signal and consistent with a Gaussian distribution with a 133 μK rms. Yahil & Vidal (1977) discuss tests of normality in another context, although in their case measurement errors were not significant, and it is unlikely that a strong result can be extracted from a low signal-to-noise ratio data set such as that of the RING. Geometrical tests of normal and non-Gaussian distributions are discussed in detail in Coles & Barrow (1987) and Coles (1988), with emphasis on measuring the statistics of hotspots. Topological methods in the context of the non-Gaussian anisotropies induced by cosmic strings are also discussed in Gott et al. (1990). Methods such as these may prove powerful if fluctuations are detected and imaged, although it is likely that incomplete sampling and nonuniform noise levels in the maps will reduce the effectiveness of these methods. Overall, the Bayesian approach appears to be the most promising. Given a set of maps generated using a specific model, the likelihood function might be constructed using Monte Carlo sampling from the realizations. In this manner, useful constraints can be placed in both Gaussian and non-Gaussian models.

6. CONCLUSIONS

The linked sampling of switched data used in the RING has proved to be a successful approach to optimizing the sensitivity and sky coverage of a many-field experiment. Most important, the interlocked geometry provides a check of the noise level and possible systematic errors. In the absence of systematic errors, and independent of any real sky fluctuations, the expected mean value of the RING fields is zero. The actual mean value -6 ± 12 μK is persuasive evidence that the data set is free from systematic offsets in the measurements. The fact that no subtraction of bias levels or gradients was used nor was required attests to the robustness of the observing procedure. The detection, identification, and successful subtraction of discrete radio sources lends confidence to the final calibration of the data, although the high level of contamination, while not surprising, makes the production of a confusion-free data set difficult.

The fluctuation level in the analysis of the RING data is in disagreement with the previous OVRO NCP limits at the 95% level, although this is marginally consistent with the increased contamination by foreground radio sources in the larger surveyed area. *The uncertainty of extrapolation of the source counts from the lower frequency VLA survey and the poor determination of the contribution of sources in the sidelobes of the OVRO beam lead us to treat the RING limits as upper limits only.* This may disappoint those eager for the detection of real cosmic background anisotropy; however, the significant possibility of foreground source contamination in the RING data requires us to adopt a conservative approach. Because large experiments such as ours can identify candidate targets for closer study, all hope is not lost for anisotropies, and indeed the RING experiment has yielded two fields for which we have scheduled deeper observations at the Owens Valley Radio Observatory. One field, which shows a 5.2 σ signal yet contains no sufficiently bright VLA sources, is a strong candidate for an interesting background fluctuation or an unusual foreground source. If observations of these fields continue to indicate a significant signal, the VLA and high-frequency measurements will discriminate between the several interesting possibilities for the nature of the objects.

Because of the problems with residual foreground contamination, the limits from the NCP experiment still place the best limits on Gaussian cosmic background fluctuation models on these angular scales. However, the RING may still provide interesting limits for some classes of non-Gaussian models. The lack of detailed and compelling non-Gaussian models in the literature leaves us with no good examples against which to test the RING data, but hopefully these will be forthcoming. The development of analytical tools to deal with non-Gaussian statistics is also needed to make use of the increased leverage of large experiments such as the RING, and the very large data sets such as those provided by the MIT balloon observations and the *COBE* satellite.

7. IMPLICATIONS OF THE *COBE* DETECTION

As announced recently (Smoot et al. 1992), analysis of the *COBE* first-year DMR data has yielded the detection of anisotropy in the microwave background radiation consistent with a scale-invariant fluctuation spectrum with an amplitude consistent with unbiased CDM models. The reader is referred to the aforementioned paper and a companion paper (Wright et al. 1992) for the detailed discussion of the results and implications for various cosmological and galaxy formation models. Using the quadrupole normalization for a Harrison-Zel'dovich spectrum given in Wright et al. (1992), Efstathiou, Bond, & White (1992) have computed limits on the linear biasing parameter b_8 (see § 5.2). Given the *COBE* measured amplitude, Efstathiou et al. find for "standard" CDM models, $b_8 \approx 0.93$ with a 1 σ range of $0.75 < b_8 < 1.22$, again consistent with an unbiased ($b_8 = 1$ model. As noted in § 5.2 and in Bond & Myers (1992), the OVRO NCP experiment places a limit of $b_8 > 0.46$ (95%) for CDM models with total $\Omega = 1$ and $\Omega_B = 0.03$ in baryons, and a limit of $b_8 > 0.68$ for $\Omega_B = 0.1$. Thus, the OVRO sensitivity is within a factor of 2 of reaching the level of fluctuations predicted for the standard CDM models given the *COBE* results. Failure to detect these anisotropies on the angular scales probed by the OVRO experiment would be evidence for nonstandard recombination. It should also be noted that intermediate angular scale observations, such as those of Meinhold & Lubin, are even closer to the predicted fluctuation levels. Thus, ground-based observations on intermediate and small angular scales should very soon begin to place strong constraints on the fluctuations measured by *COBE*.

We have interpreted the RING results as upper limits to cosmic microwave background anisotropies because of as-yet unresolved questions about discrete source confusion. If, however, we were to assume that all of the detected signal in the RING comes from microwave background fluctuations, then the values in equation (35) of $\Delta T/T \approx 3.3 \times 10^{-5}$ and limits of $2.3 \times 10^{-5} < \Delta T/T < 4.5 \times 10^{-5}$ (95%) would corre-

spond to $b_8 \approx 0.24$ and $0.17 < b_8 < 0.34$ for $\Omega_B = 0.03$ and to $b_8 \approx 0.35$ and $0.26 < b_8 < 0.50$ for $\Omega_B = 0.1$. Therefore, the amplitude of the fluctuations found in the RING experiment is larger than that expected from the models favored given the *COBE* detection, at a significance compared to the *COBE* values of 3.8 σ for $\Omega_B = 0.03$ and 3.2 σ for $\Omega_B = 0.03$. These numbers can be reconciled if there is an added source of small-scale fluctuations. These anisotropies must be significantly larger than those produced in CDM models by the quadratic Vishniac effect (Vishniac 1987; Efstathiou & Bond 1987, Efstathiou 1988). Because the range of angular scales probed by the RING experiment corresponds to the wavelengths of perturbations in the density spectrum at recombination that form structures on scales from groups to superclusters of galaxies, for which the correlation functions can be measured, any extra power on these scales would show up in galaxy and cluster correlation functions. In fact, between the very large-scale fluctuations probed by *COBE* and the small-scale fluctuations probed by galaxy surveys and the OVRO experiment, limits on the primordial fluctuation amplitude, any long spatial wavelength extension to the fluctuation spectrum, and the extent of galaxy biasing can in principle be determined. For example, using the angular correlation function of galaxies found in the APM survey (Maddox et al. 1990), models with extra large-scale power fit the data better than a standard CDM model with $b_8 \sim 1$ (Efstathiou et al. 1992). However, at the small scales probed by the OVRO experiment the extra large-scale power is not fully effective, and we would expect a *lower* signal in the RING data than that for a $b_8 = 1$ CDM model alone. Given these theoretical prejudices, as well as our observational uncertainties, we must still consider the most likely origin of the RING anisotropy to be foreground source contamination.

We thank the staff of the OVRO, especially H. Hardebeck, for keeping the maser system operating despite the many setbacks. We would also like to thank J. R. Bond for many useful discussions and the calculation of CDM predictions for the OVRO experiments. We gratefully acknowledge the support of the National Science Foundation, the James Irvine Foundation, the IBM Research Fund, and the Caltech President's Fund. This work has been supported by the National Science Foundation under grants AST 79-13249, AST 80-24119, AST 82-10259, AST 85-09822, AST 86-10693, and AST 91-19847.

REFERENCES

Albrecht, A., & Steinhardt, P. J. 1982, Phys. Rev. Lett., 48, 1220
Baars, J. W. M., Genzel, R., Pauliny-Toth, I. I. K., & Witzel, A. 1977, A&A, 61, 99
Banday, A. J., et al. 1991, ApJ, 375, 432
Banday, A. J., & Wolfendale, A. W. 1990, MNRAS, 245, 182
Berger, J. O. 1985, Statistical Decision Theory and Bayesian Analysis (New York: Springer)
Bernstein, G. M., Fischer, M. L., Richards, P. L., Petersen, J. B., & Timusk, T. 1989, ApJ, 337, L4
Birkinshaw, M. 1987, in IAU Symp. 124, Observational Cosmology, ed. A. Hewitt, G. Burbidge, & L. Z. Fang (Dordrecht: Kluwer), 83
Birkinshaw, M., Gull, S. F., & Hardebeck, H. E. 1984, Nature, 309, 34
Bond, J. R. 1988a, in NATO Summer School on the Early Universe, ed. W. G. Unruh & G. W. Semenoff (Dordrecht: Reidel), 283
———. 1988b, in The Epoch of Galaxy Formation, ed. C. S. Frenk, R. S. Ellis, T. Shanks, A. F. Heavens, & J. A. Peacock (Dordrecht: Kluwer), 211
Bond, J. R., Carr, B. J., & Hogan, C. J. 1986, ApJ, 306, 428
———. 1991a, ApJ, 367, 420
Bond, J. R., & Efstathiou, G. 1984, ApJ, 285, L45
———. 1987, MNRAS, 226, 655
Bond, J. R., Efstathiou, G., Lubin, P. M., & Meinhold, P. R. 1991b, Phys. Rev. Lett., 66, 2179
Bond, J. R., & Myers, S. T. 1992, in Trends in Astroparticle Physics, ed. D. Cline & R. Peccei (Singapore: World Scientific), 262
Bouchet, F. R., Bennett, D. P., & Stebbins, A. 1988, Nature, 335, 410
Boughn, S. P., Cheng, E. S., Cottingham, D. A., Fixsen, D. J., & Wilkinson, D. T. 1992, ApJ, 391, L49
Cole, S., & Efstathiou, G. 1989, MNRAS, 239, 195
Cole, S., & Kaiser, N. 1989, MNRAS, 233, 637
Coles, P. 1988, MNRAS, 234, 509
Coles, P., & Barrow, J. D. 1987, MNRAS, 228, 407
Condon, J. J. 1974, ApJ, 188, 279
———. 1988, in Galactic and Extragalactic Radio Astronomy, ed. G. L. Verschur & K. I. Kellermann (New York: Springer), 641
Condon, J. J., Condon, M. A., & Hazard, C. 1982, AJ, 87, 739
Cornwell, T. J. 1985, in Synthesis Imaging, Proc. NRAO Summer School, Socorro, New Mexico, ed. R. A. Perley, F. R. Schwab, & A. H. Bridle (Green Bank, WV: NRAO), 109
Daly, R. A. 1988, MNRAS, 232, 853
Danese, L., De Zotti, G., & Mandolesi, N. 1983, A&A, 121, 114
Davies, R. D., Lasenby, A. N., Watson, R. A., Daintree, E. J., Hopkins, J., Beckman, J., Sanchez-Almeida, J., & Rebolo, R. 1987, Nature, 326, 462
de Bernardis, P., et al. 1990, ApJ, 360, L31
Djorgovski, S., & Weir, N. 1990, ApJ, 351, 343
Doroshkevich, A. G., Klypin, A. A., & Khlopov, M. U. 1989, MNRAS, 239, 923
Efstathiou, G. 1988, in Large Scale Motions in the Universe, ed. V. C. Rubin & G. V. Coyne (Princeton: Princeton Univ. Press), 299
Efstathiou, G., & Bond, J. R. 1987, MNRAS, 227, 33
Efstathiou, G., Bond, J. R., & White, S. D. M. 1992, MNRAS, in press
Fomalont, E. B., Kellermann, K. I., Anderson, M. C., Weistrop, D., Wall, J. V., Windhorst, R. A., & Kristian, J. A. 1988, AJ, 96, 1187
Fomalont, E. B., Partridge, R. B., Lowenthal, J. D., & Windhorst, R. A. 1992, ApJ, submitted
Fomalont, E. B., Windhorst, R. A., Kristian, J. A., & Kellermann, K. I. 1991, AJ, 102, 1258
Franceschini, A., Toffolatti, L., Danese, L., & De Zotti, G. 1989, ApJ, 344, 35
Gott, J. R., III., Park, C., Juszkiewicz, R., Bies, W. E., Bennett, D. P., Bouchet, F. R., & Stebbins, A. 1990, ApJ, 352, 1
Gull, S. F. 1989, in Maximum Entropy and Bayesian Methods, ed. J. Skilling (Dordrecht: Kluwer), 53
Gull, S. F., & Skilling, J. 1984, IEEE Proc., 131(F), 646
Gush, H. P., Halpern, M., & Wishnow, E. 1990, Phys. Rev. Lett., 65, 537
Guth, A. H. 1981, Phys. Rev. D, 32, 347
Hauser, M. G., et al. 1984, ApJ, 278, L15
Hogan, C. J., & Bond, J. R. 1988, in The Post-Recombination Universe, ed. N. Kaiser & A. N. Lasenby (Dordrecht: Kluwer), 141
Hogan, C. J., & Partridge, R. B. 1989, ApJ, 341, L29
Holtzman, J. A. 1989, ApJS, 71, 1
Ikeuchi, S. 1981, PASJ, 33, 211
Kellermann, K. I., & Wall, J. V. 1987, in IAU Symp. 124, Observational Cosmology, ed. A. Hewitt, G. R. Burbidge, & L. Z. Fang (Dordrecht: Kluwer), 545
Kendall, M., & Stuart, A. 1977, The Advanced Theory of Statistics, Vol. 1 (4th ed.; New York: Macmillan)
———. 1979, The Advanced Theory of Statistics, Vol. 2 (4th ed.; New York: Macmillan)
Klein, M. J., & Gulkis, S. 1978, Icarus, 35, 44
Klypin, A. A., Sazhin, M. V., Strukov, I. A., & Skulachev, D. P. 1987, Soviet Astron. Lett., 13, 104
Kofman, L. A., & Pogosyan, D. Y. 1988, Phys. Lett. B, 214, 508
Kraus, J. D. 1982, Radio Astronomy (Ohio: Cygnus-Quasar)
Lawson, K. D., Mayer, C. J., Osborne, J. L., & Parkinson, M. L. 1987, MNRAS, 225, 307
Linde, A. D. 1982, Phys. Lett. B, 108, 389
Low, F. J., et al. 1984, ApJ, 278, L19
Maddox, S. J., Efstathiou, G., Sutherland, W. J., & Loveday, J. 1990, MNRAS, 242, 43P
Martin, H. M., & Partridge, R. B. 1988, ApJ, 324, 794
Mather, J. C., et al. 1990, ApJ, 354, L37
Matsumoto, T., Hayakawa, S., Matsuo, H., Murakami, H., Sato, S., Lange, A. E., & Richards, P. L. 1988, ApJ, 329, 567
Meinhold, P., & Lubin, P. 1991, ApJ, 370, L11
Meyer, S. S., Cheng, E. S., & Page, L. A. 1991, ApJ, 371, L7
Myers, S. T. 1990, Ph.D. thesis, Caltech
Ostriker, J. P., & Cowie, L. L. 1981, ApJ, 243, L127
Ostriker, J. P., & Thompson, C. 1987, ApJ, 323, L97
Ostriker, J. P., Thompson, C. J., & Witten, E. 1987, Phys. Lett. B, 180, 231
Pauliny-Toth, I. I. K., Witzel, A., Preuss, E., Baldwin, J. E., & Hills, R. E. 1978, A&AS, 34, 253

Peebles, P. J. E. 1983, ApJ, 274, 1
Press, W. H., Ryden, B. S., & Spergel, D. H. 1989, ApJ, 347, 604
Readhead, A. C. S., & Lawrence, C. R. 1992, ARA&A, 30, 653
Readhead, A. C. S., Lawrence, C. R., Myers, S. T., Sargent, W. L. W., Hardebeck, H. E., & Moffett, A. T. 1989, ApJ, 346, 566 (Paper I)
Ryu, D., Vishniac, E. T., & Chiang, W. 1990, ApJ, 354, 389
Salopek, D. S. 1991, in Proc. 4th Canadian Conference on General Relativity and Relativistic Astrophysics, ed. G. Kunstatter (Singapore: World Scientific), in press
Salopek, D. S., Bond, J. R., & Bardeen, J. M. 1989, Phys. Rev. D. 40, 1753
Schaefer, R. K., Shafi, Q., & Stecker, F. W. 1989, ApJ, 347, 575
Schaeffer, R., & Silk, J. 1988, ApJ, 333, 509
Skilling, J. 1989, in Maximum Entropy and Bayesian Methods, ed. J. Skilling (Dordrecht: Kluwer)
Smoot, G. F., et al. 1991, ApJ, 371, L1
———. 1992, ApJ, 396, L1
Sunyaev, R. A., & Zel'dovich, Y. B. 1981, Ap&SS, 1 (E), 1
Timbie, P. T., & Wilkinson, D. T. 1988, Rev. Sci. Instr., 59, 914
———. 1990, ApJ, 353, 140
Turok, N. 1989, Phys. Rev. Lett., 63, 2624
Uson, J. M., & Wilkinson, D. T. 1984a, ApJ, 277, L1
———. 1984b, ApJ, 283, 471
———. 1984c, Nature, 312, 427
Vilenkin, A. 1986, in Inner Space/Outer Space, ed. E. W. Kolb, M. S. Turner, D. Lindley, K. Olive, & D. Seckel (Chicago: Univ. Chicago Press), 269
Vishniac, E. T. 1987, ApJ, 322, 597
Vittorio, N., Meinhold, P., Muciaccia, P. F., Lubin, P., & Silk, J. 1991, ApJ, 372, L1
Vittorio, N., & Silk, J. 1984, ApJ, 285, L39
Wall, J. V., Scheuer, P. A. G., Pauliny-Toth, I. I. K., & Witzel, A. 1982, MNRAS, 198, 221
Windhorst, R., et al. 1992, AJ, submitted
Wise, M. B. 1988, in NATO Summer School on the Early Universe, ed. W. G. Unruh & G. W. Semenoff (Dordrecht: Reidel), 215
Wright, E. L., et al. 1991, ApJ, 381, 200
———. 1992, ApJ, 396, L13
Yahil, A., & Vidal, N. V. 1977, ApJ, 214, 347